UNPUBLISHED PRELIMINARY DATA

THE ANTENNA LABORATORY

RESEARCH ACTIVITIES in --

Automatic Controls — *Antennas* — *Echo Area Studies*
Microwave Circuits — *Astronautics* — *E M Field Theory*
Terrain Investigations — *Radomes* — *Systems Analysis*
Wave Propagation — *Submillimeter Applications*

Radiation Characteristics of a Planar Broadside Array of Directive Elements

by

Joseph A. Kinzel

Grant Number NsG-448

1691-6 15 April 1964

Prepared for:
National Aeronautics and Space Administration
Washington 25, D.C.

Department of ELECTRICAL ENGINEERING

THE OHIO STATE UNIVERSITY
RESEARCH FOUNDATION
Columbus, Ohio

NOTICES

When Government drawings, specifications, or other data are used for any purpose other than in connection with a definitely related Government procurement operation, the United States Government thereby incurs no responsibility nor any obligation whatsoever, and the fact that the Government may have formulated, furnished, or in any way supplied the said drawings, specifications, or other data, is not to be regarded by implication or otherwise as in any manner licensing the holder or any other person or corporation, or conveying any rights or permission to manufacture, use, or sell any patented invention that may in any way be related thereto.

The Government has the right to reproduce, use, and distribute this report for governmental purposes in accordance with the contract under which the report was produced. To protect the proprietary interests of the contractor and to avoid jeopardy of its obligations to the Government, the report may not be released for non-governmental use such as might constitute general publication without the express prior consent of The Ohio State University Research Foundation.

Qualified requesters may obtain copies of this report from the Defense Documentation Center, Cameron Station, Alexandria, Virginia. Department of Defense contractors must be established for DDC services, or have their "need-to-know" certified by the cognizant military agency of their project or contract.

REPORT 1691-6

REPORT

by

THE OHIO STATE UNIVERSITY RESEARCH FOUNDATION
COLUMBUS, OHIO 43212

Sponsor	National Aeronautics and Space Administration Washington 25, D.C.
Grant Number	NsG-448
Investigation of	Spacecraft Antenna Problems
Subject of Report	Radiation Characteristics of a Planar Broadside Array of Directive Elements
Submitted by	Joseph A. Kinzel Antenna Laboratory Department of Electrical Engineering
Date	15 April 1964

The material contained in this report is also used as a thesis submitted to the Department of Electrical Engineering The Ohio State University as partial fulfillment for the degree Master of Science.

ACKNOWLEDGMENTS

The author wishes to express his sincere appreciation for the suggestions, encouragement, and guidance extended him by his advisor, Professor Curt A. Levis. My thanks go also to Professor C.H. Walter, Professor C.T. Tai, and the other members of the Antenna Laboratory who have aided me in numerous ways.

CONTENTS

LIST OF TABLES

LIST OF ILLUSTRATIONS

LIST OF ILLUSTRATIONS(Cont.)

LIST OF ILLUSTRATIONS(Cont.)

CHAPTER I
INTRODUCTION

The directivity of antenna arrays consisting of isotropic sources is firmly established [1-5]. A fairly complete set of curves showing the directivity of uniform linear arrays of isotropic sources and dipoles as a function of the element spacing has been prepared by Tai [1], but to the author's knowledge no definite criterion for the optimum spacing of directive sources in a planar array has been worked out. Utilizing an array configuration which is not linear and introducing elements whose radiation pattern is dependent on the polar angle greatly complicates the integral expression for the power radiated from the antenna array and therefore complicates directivity computations.

Planar broadside arrays of individually directive endfire elements are becoming increasingly popular since, with them, it is possible to obtain the directivity necessary for tracking space vehicles. Also, since very directive antennas on the ground and on the vehicles, are required for communicating with deep-space probes, such arrays might be considered for this application. It therefore becomes important that a criterion be developed for the optimum spacing of the elements in such an array. One criterion

which has been applied is that of converting the directivity of an array element to an effective aperture and spacing the elements accordingly. This has been done purely on a heuristic basis.

This work is directed towards the exploration of this "aperture concept" by using as an example the four-element planar broadside array shown in Fig. 1. This particular array is used because of several inherent advantages. With directive elements the array is reasonably independent of the azimuthal angle. The array configuration also provides a convenient method, mechanically, for varying the element spacing and allowing the elements to be spaced as compactly as desired. Four elements are the minimum number that can form a planar array, and the geometry shown and circular polarization were chosen for symmetry considerations.

The theoretical results for directivity, using the function $\cos^{n}\theta$ to approximate the individual element sources, are obtained. By varying the parameter n it is possible to simulate endfire element patterns of any desired directivity. Experimental radiation patterns are then obtained for an array of helices having the geometry of Fig. 1 for various spacings of the three peripheral elements with respect to the middle element. These patterns are then shown to agree with array patterns calculated by multiplying the pattern of the individual element by the theoretical array factor

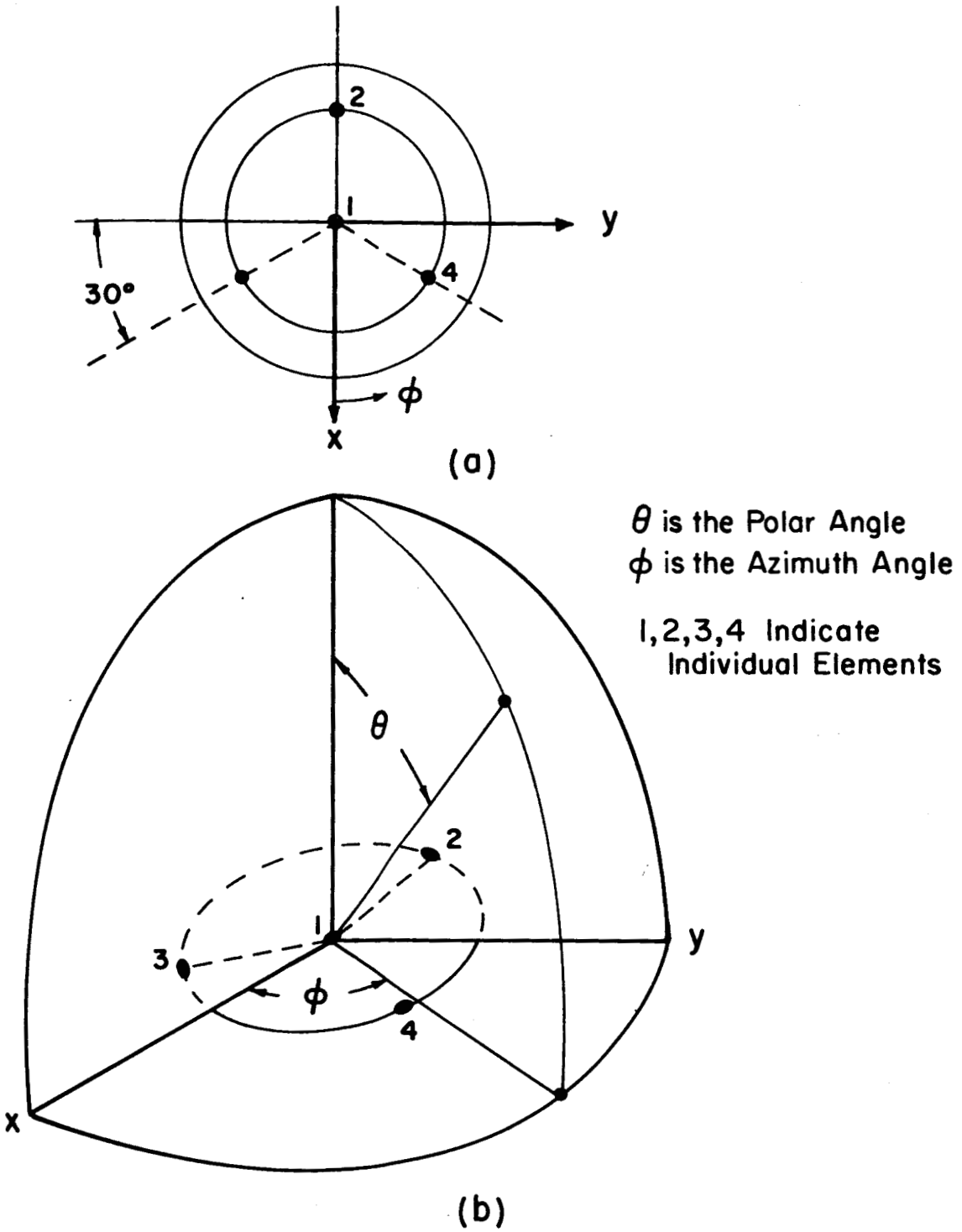

Fig. 1. The four-element planar array and the appropriate coordinate system
(a) Azimuth plane
(b) Three dimensional view.

(that pattern obtained by substituting isotropic sources for the array elements).

The following conclusions emerge from this investigation. According to the calculations, the "aperture-concept", i.e., spacing directive elements by the diameter of the circle which represents the equivalent aperture, results in a near-optimum design in the sense that greater spacings would produce little increase in total directivity and lesser spacings would decrease directivity substantially. Secondly, the measured patterns agreed with those calculated by pattern multiplication for spacings greater than 1.2 wavelengths. This was to be expected since the pattern of each element was relatively unaffected by neighboring elements; however the agreement was surprisingly good even at close spacings where the pattern of one element was grossly distorted by the presence of other elements even when these were open-circuited at the terminal, in which case pattern multiplication would not be expected to give good results.

In the experimental part of this investigation, it was necessary to probe the terminal currents of the individual elements. The difficulties associated with this measurement will be discussed along with the observed effect of close spacing on the radiation pattern. Finally the effect of winding the individual helices around polystyrene tubing will be mentioned.

In all the calculations and in all the experimental work each peripheral helix is spaced the same distance from the center helix and the four helices are orientated in a similar manner, as shown in Fig. 2.

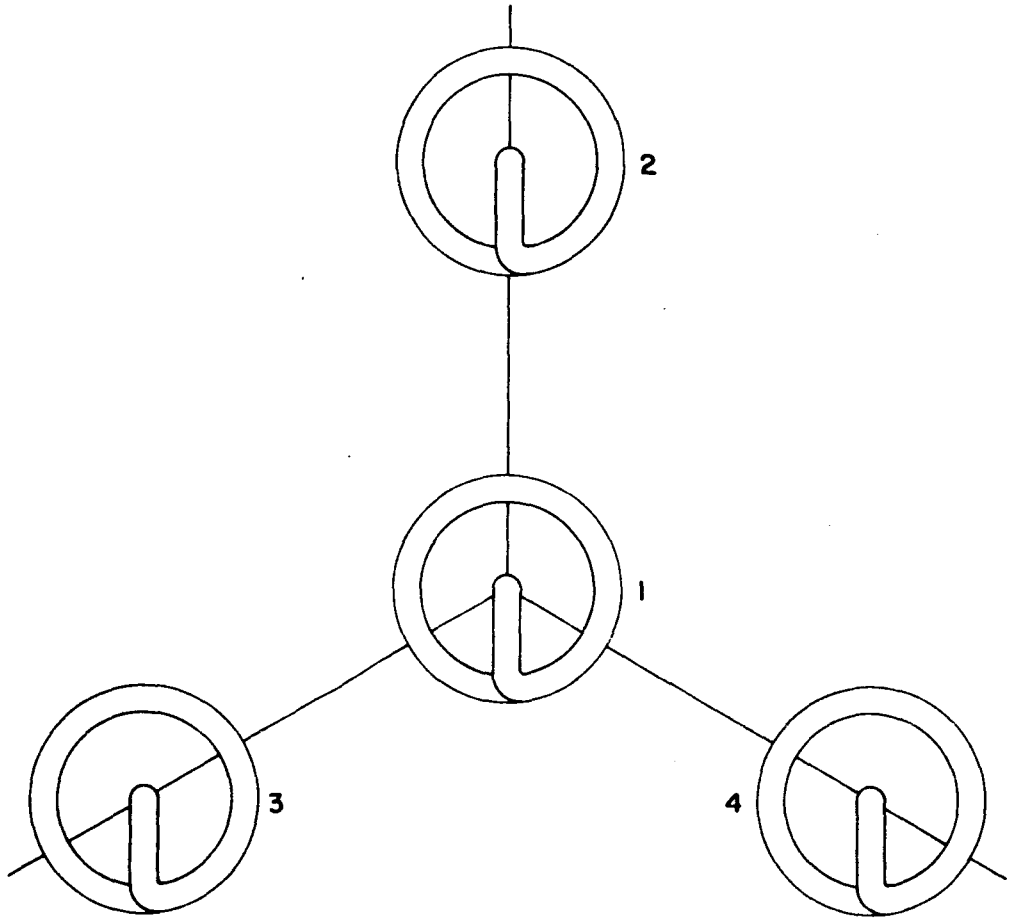

Fig. 2. Relative orientation of helices.

CHAPTER II
DIRECTIVITY CALCULATION OF THE FOUR-ELEMENT PLANAR ARRAY

1. Obtaining the Directivity in Integral Form

We desire to calculate the directivity of the planar array of Fig. 1 where we will assume all four elements are excited by currents of equal amplitude and phase.

Directivity can be defined as[6]

$$(1\text{-}1) \qquad D_{\theta_o,\phi_o} = \frac{(\text{radiation intensity})_{\theta_o\phi_o}}{\text{average radiation intensity}}$$

where (θ_o, ϕ_o) indicates the direction in which we are considering the directivity and radiation intensity is the power radiated into the far field per unit solid angle. For the case where the individual elements are linearly or circularly polarized (1-1) can be expressed as[7]

$$(1\text{-}2) \qquad D_{\theta_o,\phi_o} = \frac{4\pi\, f(\theta_o,\phi_o)}{\int_o^{2\pi}\int_o^{\pi} f(\theta,\phi)\,\sin\theta\, d\theta\, d\phi}$$

where $f(\theta,\phi) = E(\theta,\phi)\, E(\theta,\phi)^*$ and $E(\theta,\phi)$ is a phasor quantity equal to the magnitude of one component of the electric field intensity in the far field and $E(\theta,\phi)^*$ is the complex conjugate of $E(\theta,\phi)$.

Now consider Fig. 3 where the angles and distances necessary for determining $E(\theta, \phi)$ are defined. Considering the geometry involved in Fig. 3, remembering all elements are equally excited, and utilizing pattern multiplication we may write

$$(1\text{-}3) \qquad E_t(\theta, \phi) = \frac{k}{r} \cos^{n}\theta \left[\sum_{n=1}^{4} e^{-j\beta r_n} \right],$$

where

$$\beta = \frac{2\pi}{\lambda} \quad ,$$

λ = wavelength,

k = constant,

$r_n = r_1 - d \cos \psi_n$; n = 2, 3, 4, and

d is the spacing between a peripheral element and the center element.

Now defining $g = \beta d$ and observing that $\cos \psi_n = \sin \theta \cos(\phi - \alpha_n)$ where $\alpha_2 = 180^\circ$, $\alpha_3 = 300^\circ$, $\alpha_4 = 60^\circ$ (see Fig. 3), Eq. (1-3) can be written as

$$(1\text{-}4) \qquad E_t = \frac{k}{r} \, e^{-j\beta r_1} \, \cos^{n}\theta \left[1 + \sum_{n=2}^{4} e^{+jg \sin\theta \cos(\phi - \alpha_n)} \right].$$

Defining $E(\theta, \phi)$ to equal $E_t \Big/ \left(\frac{k}{r} \, e^{-j\beta r_1} \right)$ we have

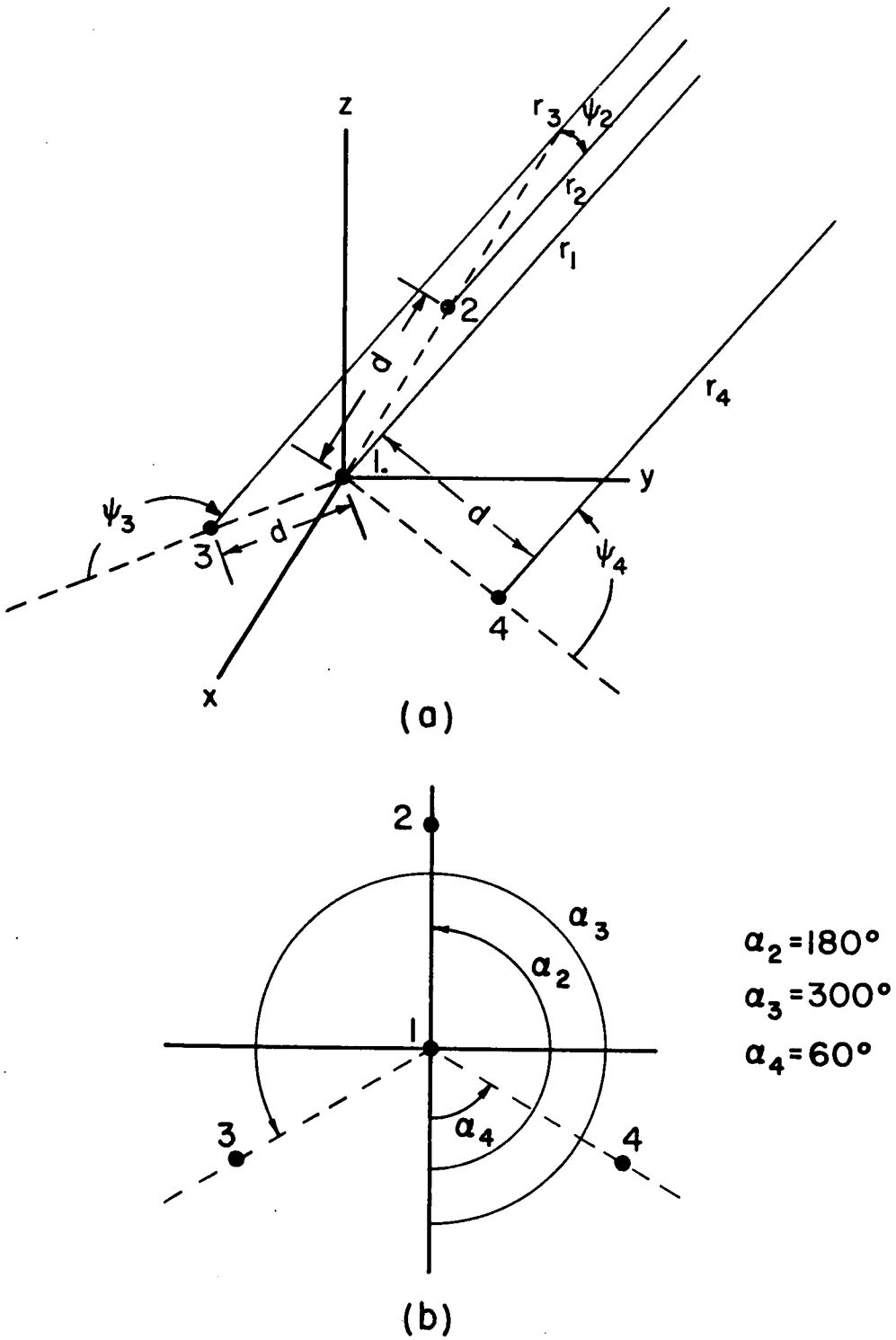

Fig. 3. Geometry defining (a) r_n and ψ_n, (b) α_n.

$$(1\text{-}5) \qquad E(\theta,\phi) = \cos^{n}\theta \left[1 + \sum_{n=2}^{4} e^{+jg \sin\theta \cos(\phi-\alpha_n)}\right] .$$

From (1-5)

$$(1\text{-}6) \qquad E(\theta,\phi)E(\theta,\phi)^* = \cos^{2n}\theta \left[1 + \sum_{n=2}^{4} e^{+jg \sin\theta \cos(\phi-\alpha_n)}\right] \cdot \left[1 + \sum_{m=2}^{4} e^{-jg \sin\theta \cos(\phi-\alpha_m)}\right]$$

which equals

$$(1\text{-}7) \qquad \cos^{2n}\theta \left\{1 + 2\sum_{n=2}^{4} \cos(g \sin\theta \cos(\phi-\alpha_n)) + \sum_{n=2}^{4}\sum_{m=2}^{4} e^{jg \sin\theta(\cos(\phi-\alpha_m)-\cos(\phi-\alpha_n))}\right\} .$$

Equation (1-7), after suitable algebraic manipulation (see Appendix A) can be expressed as

$$(1\text{-}8) \qquad E(\theta,\phi)\,E(\theta,\phi)^* = \cos^{2n}\theta \left\{4 + 2\cos(g \sin\theta\cos\phi) + 4\cos\left(\frac{g}{2}\sin\theta\cos\phi\right)\cos\left(\frac{\sqrt{3}}{2} g \sin\theta\sin\phi\right) + 4\cos\left(\frac{3g}{2}\sin\theta\cos\phi\right)\cos\left(\frac{\sqrt{3}}{2} g \sin\theta\sin\phi\right) + 2\cos(\sqrt{3}g \sin\theta\sin\phi)\right\} .$$

Now observing that (1-2) can be written as

$$(1\text{-}9) \qquad D_{\theta_o\phi_o} = \frac{4\pi\, E(\theta_o,\phi_o)\, E(\theta_o,\phi_o)^*}{\int_o^{2\pi}\int_o^{\pi} [\, E(\theta,\phi)E(\theta,\phi)^* \sin\theta]\; d\theta\, d\phi}$$

which equals

$$(1\text{-}10) \qquad \frac{4\pi\, E(\theta_o,\phi_o)\, E(\theta_o,\phi_o)^*}{\int_o^{\pi}\left[\int_o^{2\pi} E(\theta,\phi)\, E(\theta,\phi)^*\, d\phi\right] \sin\theta\, d\theta} \quad ,$$

we substitute (1-8) into (1-10) and perform the ϕ integration. The result of this integration (see Appendix B) is

$$(1\text{-}11) \quad D(\theta_o,\phi_o) = \frac{4\pi\, E(\theta_o,\phi_o)\, E(\theta_o,\phi_o)^*}{2\pi\int_o^{\pi}\left\{\left[4 + 6J_o(g\sin\theta) + 6J_o(\sqrt{3}\, g\, \sin\theta)\right]\cos^{2n}\theta\, \sin\theta\right\} d\theta} \quad ,$$

where J_o is the zero-th order Bessel function of the first kind.

For the array to be broadside we must take $\theta_o = 0^o$, and if we assume that a perfectly conducting ground plane is positioned at $\theta = 90^o$, the fields in the region $\frac{\pi}{2} \leq \theta \leq \pi$ vanish; the corresponding equation for directivity then is

$$(1\text{-}12) \quad D = \frac{16}{\int_o^{\pi/2}\left\{\left[2 + 3J_o(g\sin\theta) + 3J_o(\sqrt{3}\, g\, \sin\theta)\right]\cos^{2n}\theta \sin\theta\right\} d\theta} \quad .$$

2. Integration with Respect to the Polar Angle

In this section we will evaluate the expression for directivity as given by (1-12) which entails an integration of the form

$$(2\text{-}1) \qquad \int_0^{\pi/2} \left[J_0(g \sin\theta) \cos^{2n}\theta \sin\theta \right] d\theta .$$

It is possible to integrate (2-1) exactly, obtaining a series solution, but for element spacing of interest in this paper the series solution converged too slowly. Since the series solution would be useful for smaller spacing it has been included as Appendix C. The integration of (2-1) was performed numerically, using an IBM 7094 computer.

In order to integrate (2-1) numerically, several formulas are readily available and applicable for use on a high-speed computer. For this particular integral, involving a Bessel function, it was desirable to obtain an accurate answer with a minimum number of sample points because of the time involved in using the Bessel-function subroutine. Consequently a Gaussian Quadrature formula[8, 9] was used instead of the more common Newton-Cotes formulas. A description of these two formulas and other numerical integration formulas and their application to the integration of antenna patterns is discussed by Allen[10]. One can conclude from his work

that the Gaussian Quadrature formula is more accurate and more economical than the Newton-Cotes formula for this purpose.

The Gaussian Quadrature formulas are derived from unassigned sample points and weights which are published for the integration interval (-1 to 1)[11] . In order to use these sample points and weights it is necessary to make a change of variable in (2-1). The integral (2-1) was split into two integrals, one ranging from 0 to $\pi/4$ and the other from $\pi/4$ to $\pi/2$ to extend the 15-point Gaussian Quadrature formula to 30 points; the 30 points being sufficient to sample (2-1) by finite sums. Dividing the interval (0 to $\pi/2$) and making the change of variable

$$\theta = \frac{b-a}{2} X + \frac{b+a}{2} \quad , \tag{2-2}$$

where b is the upper limit on the integral to be evaluated and a is the lower limit, we have

$$\int_0^{\pi/2} [\, J_0(g \sin\theta) \cos^{2n}\theta \sin\theta]\, d\theta = \tag{2-3}$$

$$\frac{\pi}{8} \int_{-1}^{1} \left[J_0\left(g \sin\left(\frac{\pi}{8}X + \frac{\pi}{8}\right)\right) \sin\left(\frac{\pi}{8}X + \frac{\pi}{8}\right) \cos^{2n}\left(\frac{\pi}{8}X + \frac{\pi}{8}\right) \right.$$

$$\left. + J_0\left(g \sin\left(\frac{\pi}{8}X + \frac{3\pi}{8}\right)\right) \sin\left(\frac{\pi}{8}X + \frac{3\pi}{8}\right) \cos^{2n}\left(\frac{\pi}{8}X + \frac{3\pi}{8}\right) \right] dX.$$

It follows in the same way that

$$\int_0^{\pi/2} J_0(\sqrt{3}g \sin\theta) \cos^{2n}\theta \sin\theta\, d\theta = \tag{2-4}$$

(2-4) cont.
$$\frac{\pi}{8}\int_{-1}^{1}\left[J_o\left(\sqrt{3}g\sin\left(\frac{\pi}{8}X+\frac{\pi}{8}\right)\right)\sin\left(\frac{\pi}{8}X+\frac{\pi}{8}\right)\cos^{2n}\left(\frac{\pi}{8}X+\frac{\pi}{8}\right)+\right.$$
$$\left.J_o\left(\sqrt{3}g\sin\left(\frac{\pi}{8}X+\frac{3\pi}{8}\right)\right)\sin\left(\frac{\pi}{8}X+\frac{3\pi}{8}\right)\cos^{2n}\left(\frac{\pi}{8}X+\frac{3\pi}{8}\right)\right]dX.$$

The expression for directivity (1-12), after substituting (2-3) and (2-4), and noting that $\int_o^{\pi/2} 2\cos^{2n}\theta\sin\theta = \frac{2}{2n+1}$, is of the following form

(2-5)
$$D=\frac{16}{\frac{2}{2n+1}+\frac{3\pi}{8}\int_{-1}^{1}\left\{\sin\left(\frac{\pi}{8}X+\frac{\pi}{8}\right)\cos^{2n}\left(\frac{\pi}{8}X+\frac{\pi}{8}\right)\right.}$$
$$\left[J_o\left(g\sin\left(\frac{\pi}{8}X+\frac{\pi}{8}\right)\right)+J_o\left(\sqrt{3}g\sin\left(\frac{\pi}{8}X+\frac{\pi}{8}\right)\right)\right]$$
$$+\sin\left(\frac{\pi}{8}X+\frac{3\pi}{8}\right)\cos^{2n}\left(\frac{\pi}{8}X+\frac{3\pi}{8}\right)\left[J_o\left(g\sin\left(\frac{\pi}{8}X+\frac{3\pi}{8}\right)\right)\right.$$
$$\left.\left.+J_o\left(\sqrt{3}g\sin\left(\frac{\pi}{8}X+\frac{3\pi}{8}\right)\right)\right]\right\}dX.$$

3. Results of the Numerical Integration

The directivity of the four element planar array (as given by Eq. (2-5) was numerically evaluated for values of n = 0, 1, 2, 3, 4, 8, 12, 16, 20 as a function of the element spacing. A description of the computer program can be found in Appendix D. The results of this directivity calculation are shown in Figs. 4-12. In viewing the curves one should remember that the array elements are mounted on a perfectly conducting ground plane and that the individual element

has an electric-field radiation pattern of $\cos^{n}\theta$, resulting in a $\cos^{2n}\theta$ power pattern.

A detailed discussion of the directivity calculations is presented in Chapter IV, but it seems appropriate at this time to comment briefly on some aspects of the curves of Figs. 4-12. For zero spacing, the directivity is the same as that of a single element positioned over a ground plane, viz. 2(2n+1). As the element spacing becomes very large, sufficient that mutual impedances are negligible, the directivity must be 4 times that of a single element (since we have 4 in-phase elements with equal excitations); all of the directivity curves do approach this value. The curves also assume the patterns of an individual element is the same regardless of whether the element is isolated or is in the presence of other elements of the array. It will be shown in Chapter III that by making the last assumption, good agreement was obtained between array calculations and array patterns. But it will also be demonstrated from direct measurement of the individual element patterns that for some spacings this assumption was, in fact, incorrect even though its use led to patterns which agreed with experiment.

A final pertinent comment involves the accuracy of such a numerical integration. A direct evaluation of the error is very difficult but the following argument gives strong support to the validity of the results. For the special case where n = 0, Eq. (1-12) reduces to

$$(3\text{-}1) \qquad D = \frac{16}{2 + 3\left[\frac{\sin g}{g} + \frac{\sin \sqrt{3}\, g}{\sqrt{3}\, g}\right]} \; .$$

It is relatively simple to evaluate (3-1) by a desk calculator and the result can then be compared to the computer results for n = 0 (isotropic sources). This is a strong check on the automatic computation since the computer program has to evaluate the Bessel function and the sine function for each sample point for this special value of n precisely in the same way as for other values of n. Table I compares the results obtained with the computer for n = 0 with the results obtained from using (3-1). The results show the Gaussian Quadrature formula has provided a very accurate determination of the integral. No value is given for d = 0 since the Bessel function subroutine can not be used for an argument of zero.

TABLE I

Evaluation of Directivity Expression for n = 0

Element Spacing in Wavelengths	Directivity	
	Desk Calculator	Computer
0	2.000	-
0.2	2.961	2.961
0.4	7.780	7.780
0.6	9.730	9.730
0.8	9.643	9.643
1.0	9.270	9.270
1.2	6.433	6.433
1.4	6.987	6.987
1.6	9.674	9.674
1.8	8.644	8.644
2.0	7.879	7.879
2.2	7.655	7.655
2.4	7.231	7.231
2.6	8.466	8.466
2.8	9.101	9.101
3.0	7.668	7.668

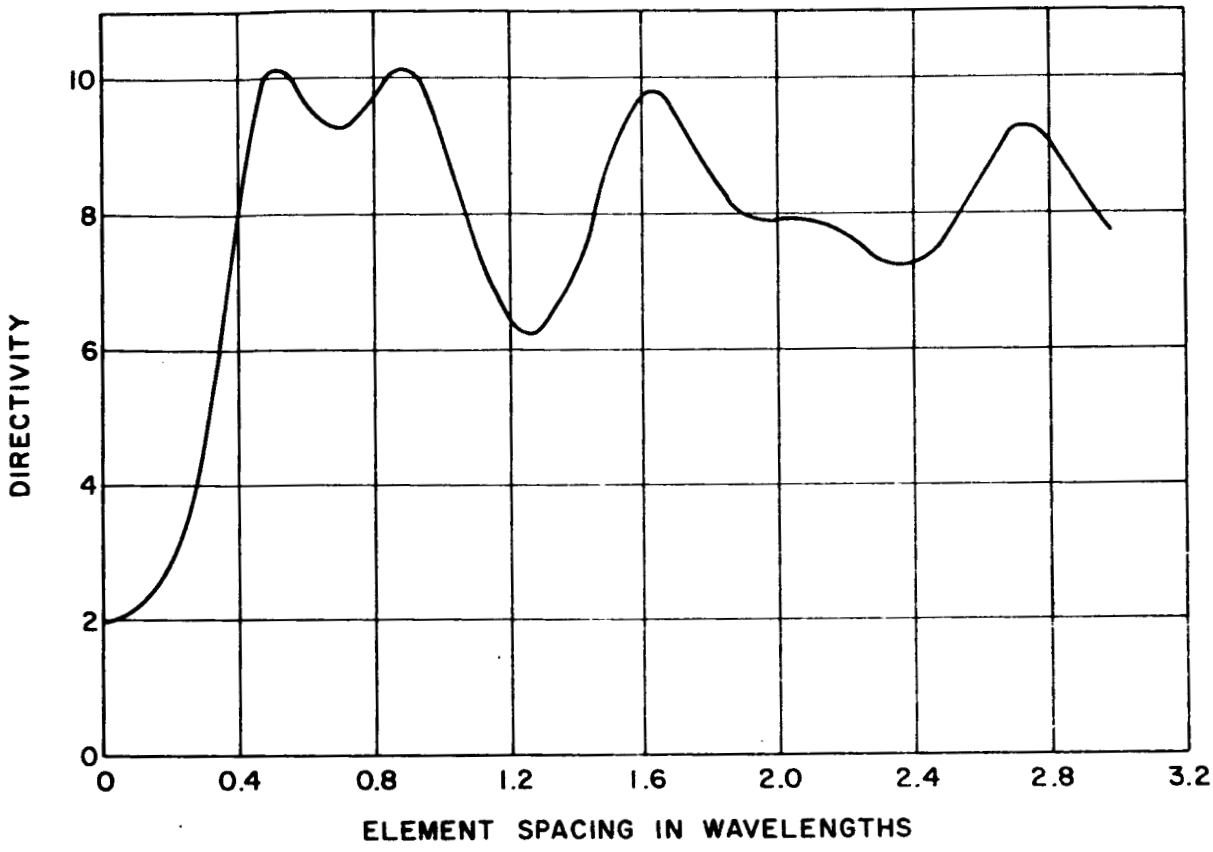

Fig. 4. Directivity of planar array of isotropic sources above a ground plane.

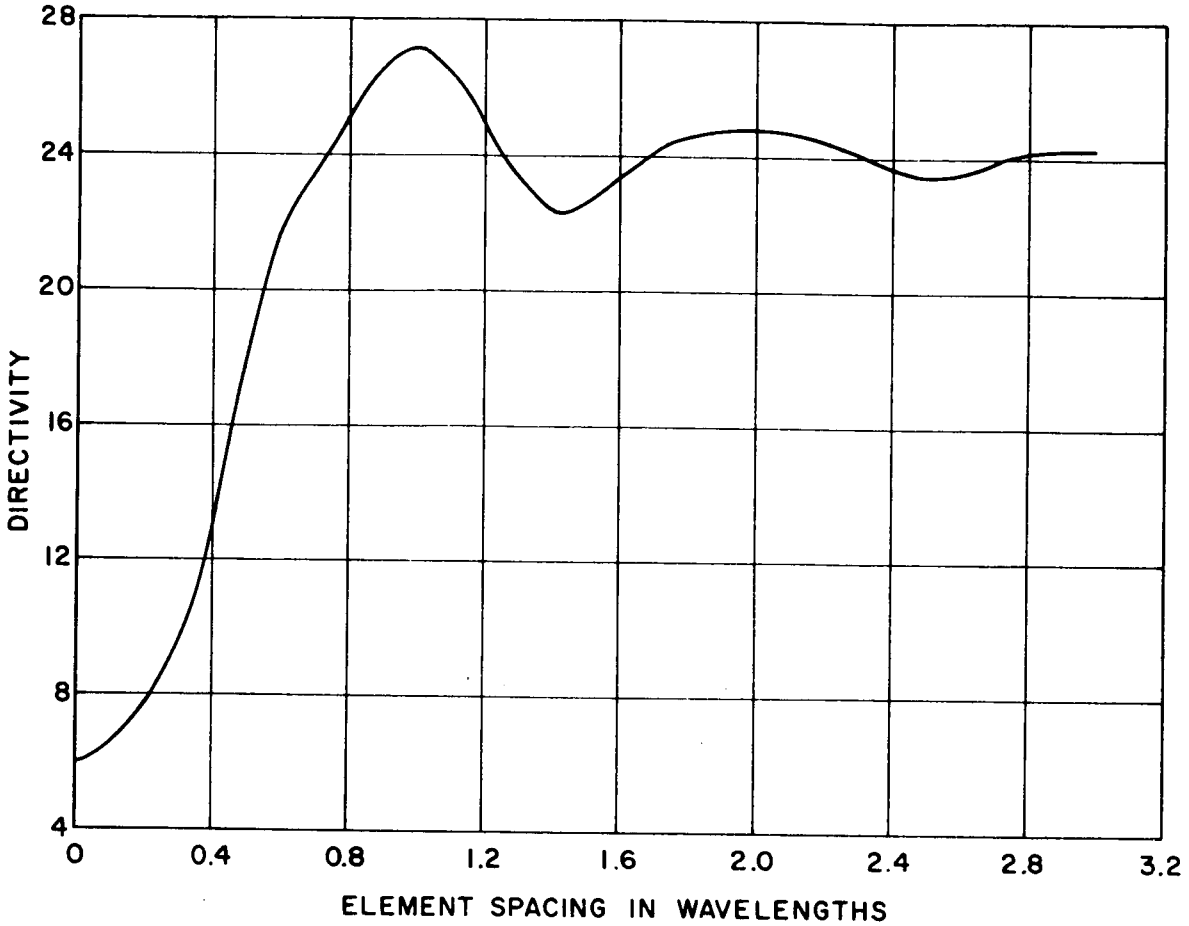

Fig. 5. Directivity of planar array of elements with cos θ voltage pattern.

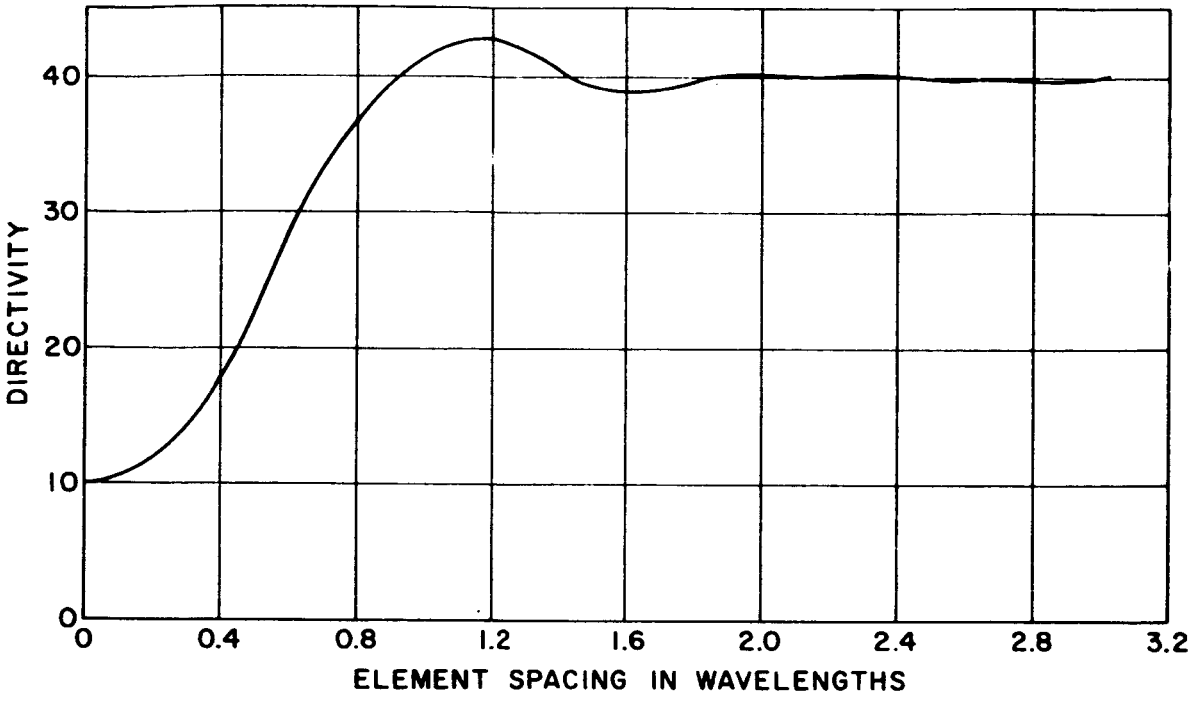

Fig. 6. Directivity of planar array of elements with $\cos^2\theta$ voltage pattern.

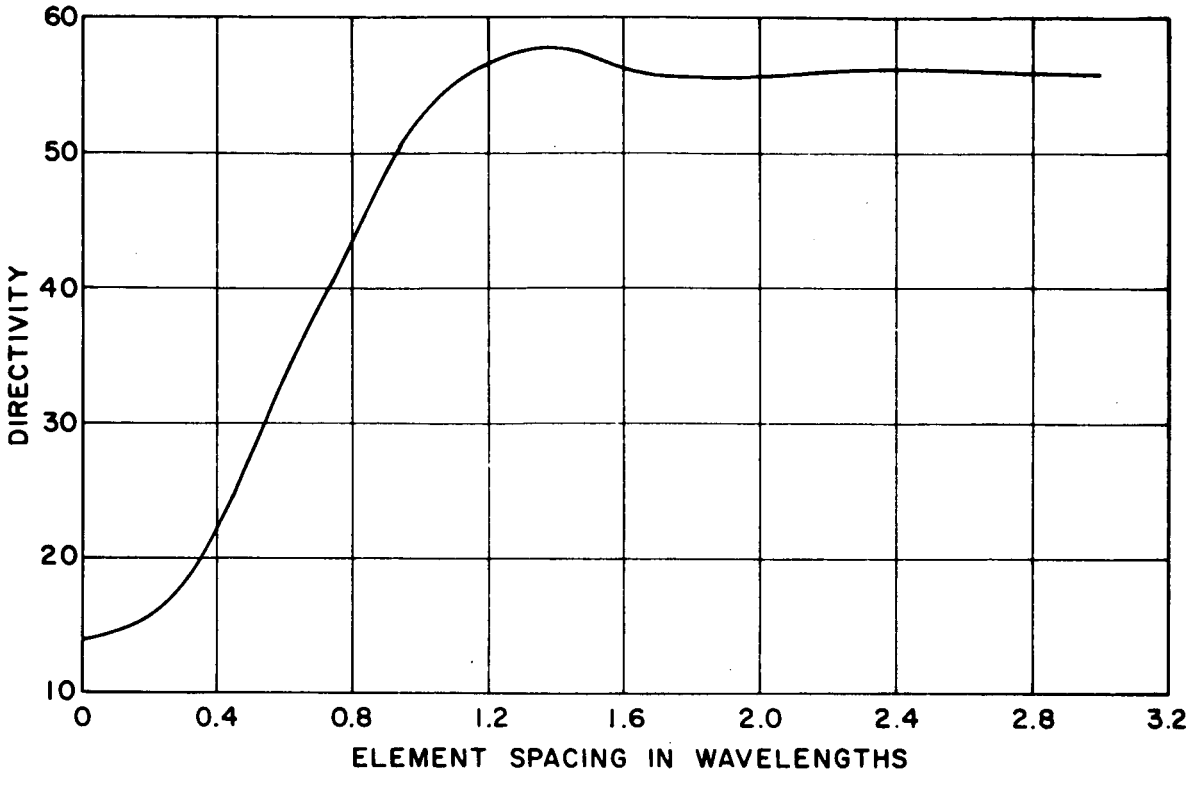

Fig. 7. Directivity of planar array of elements with $\cos^3\theta$ voltage pattern.

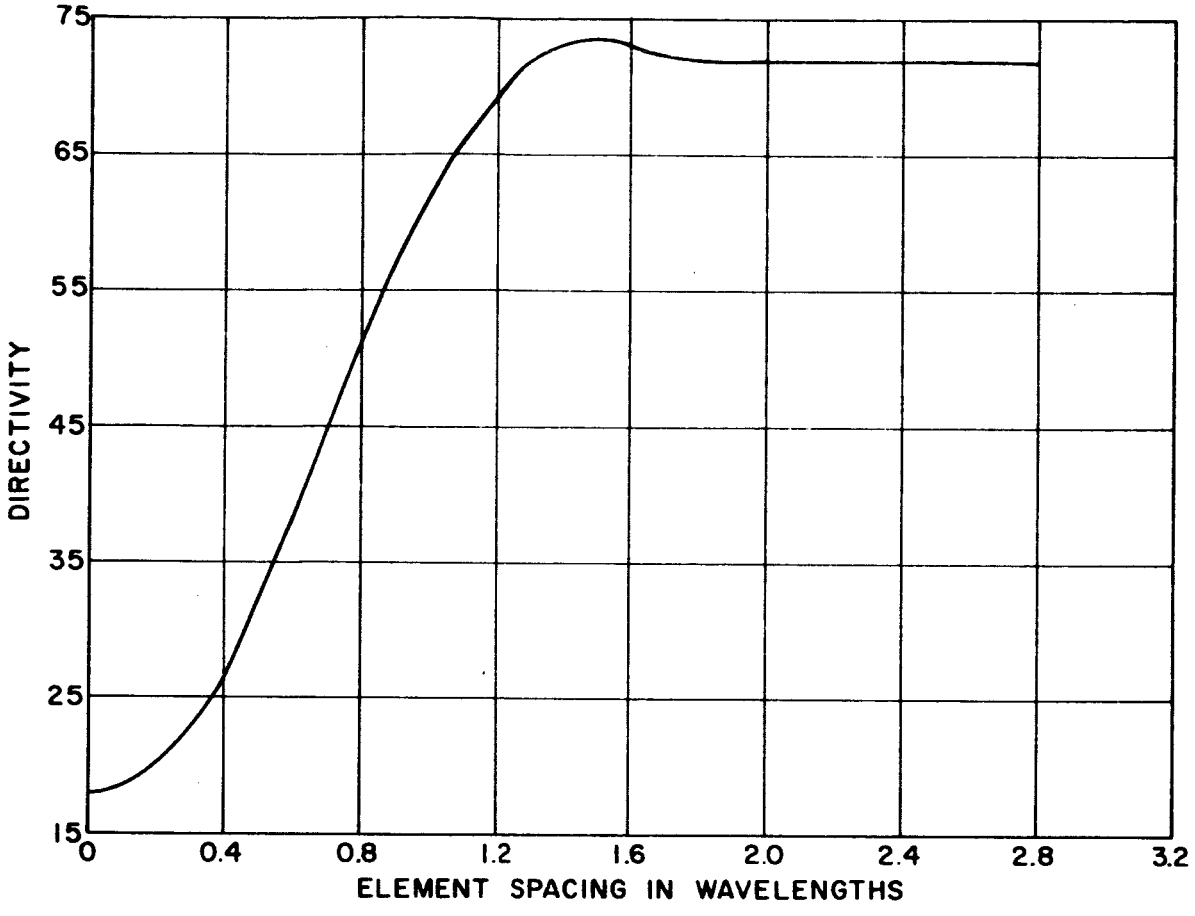

Fig. 8. Directivity of planar array of elements with $\cos^4\theta$ voltage pattern.

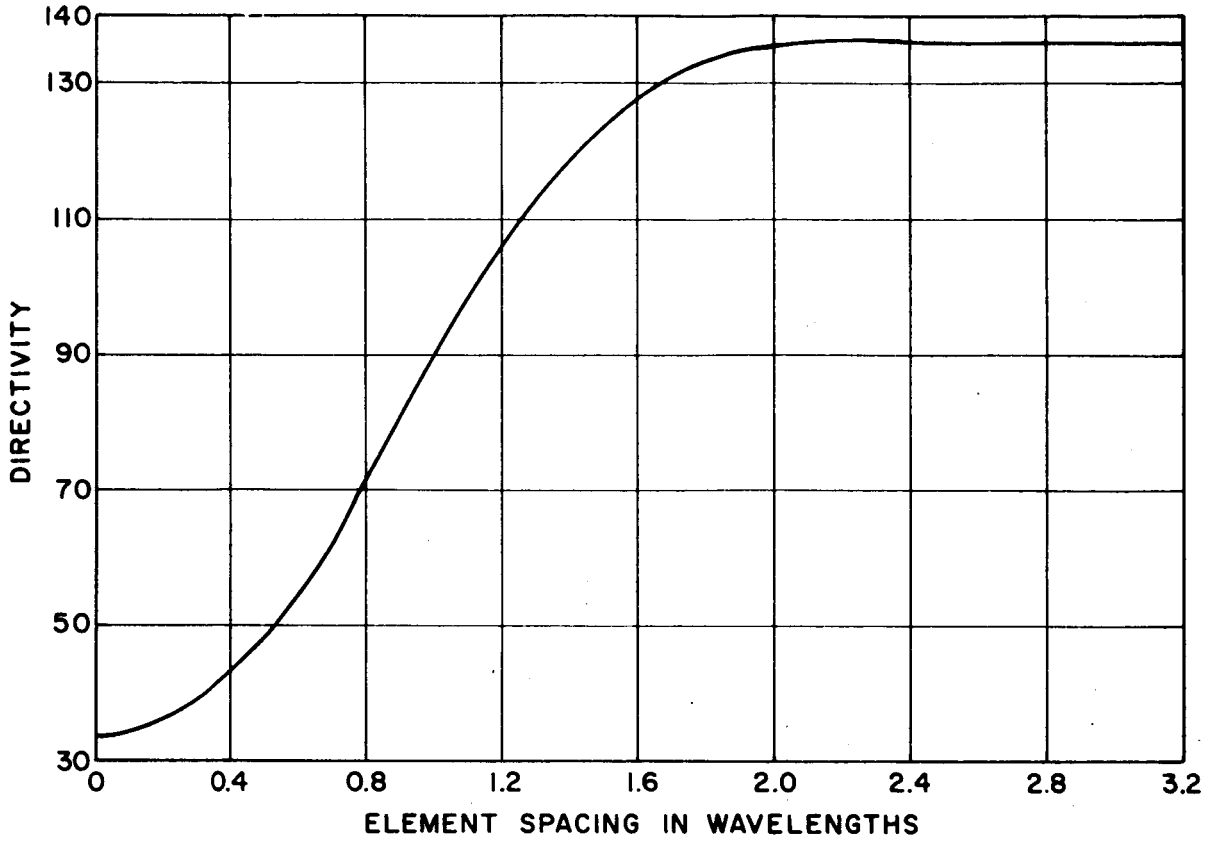

Fig. 9. Directivity of planar array of elements with $\cos^8\theta$ voltage pattern.

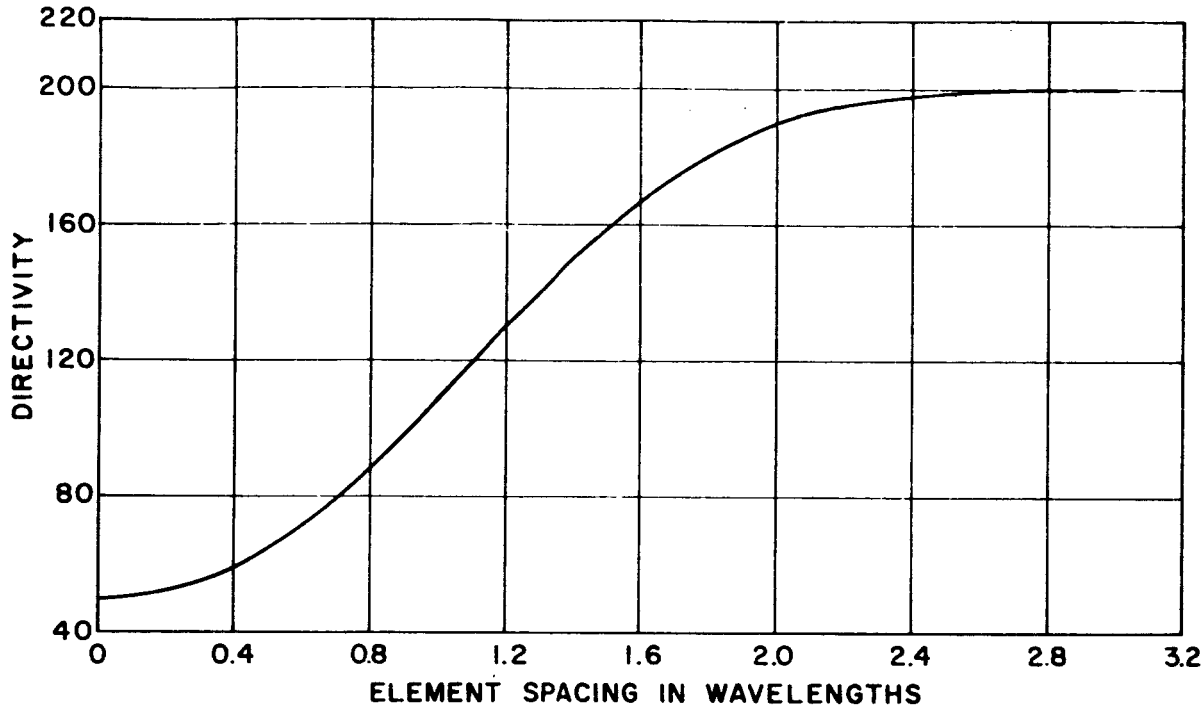

Fig. 10. Directivity of planar array of elements with $\cos^{12}\theta$ voltage pattern.

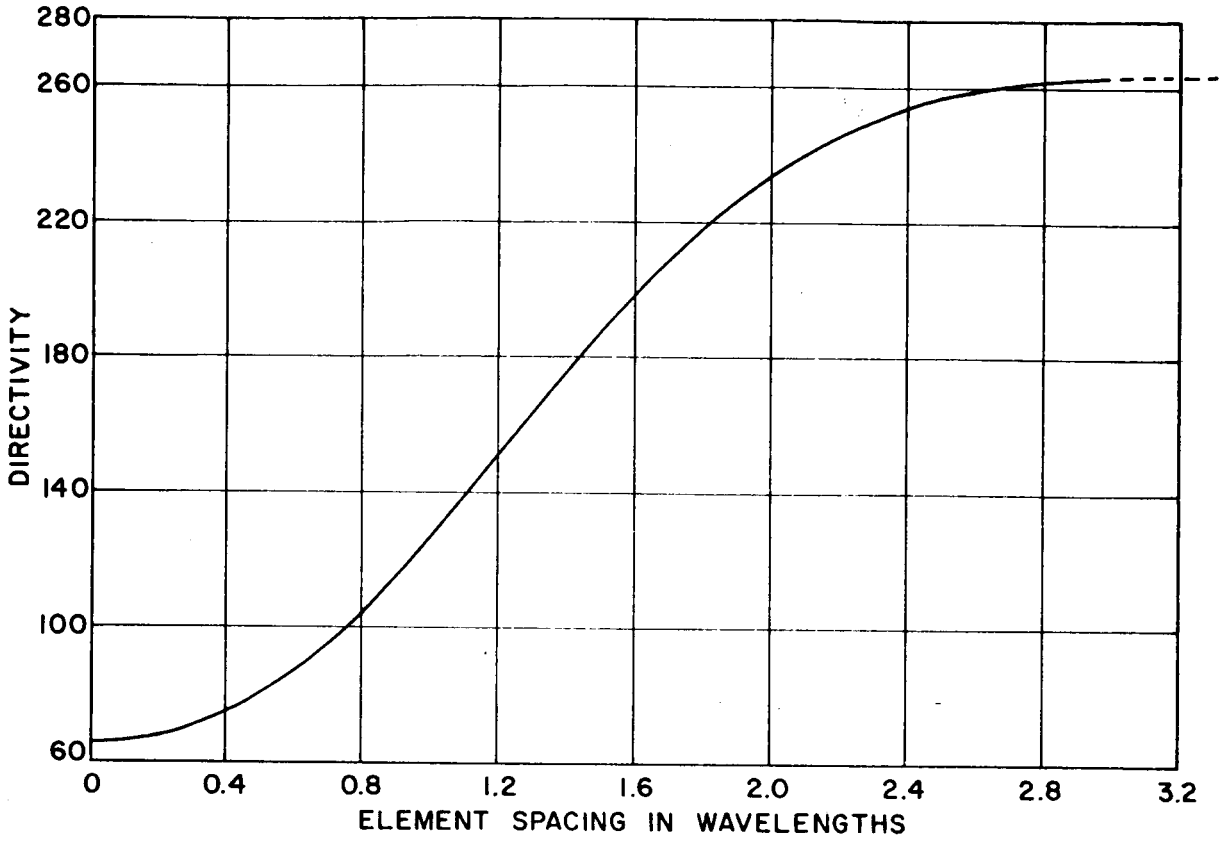

Fig. 11. Directivity of planar array of elements with $\cos^{16}\theta$ voltage pattern.

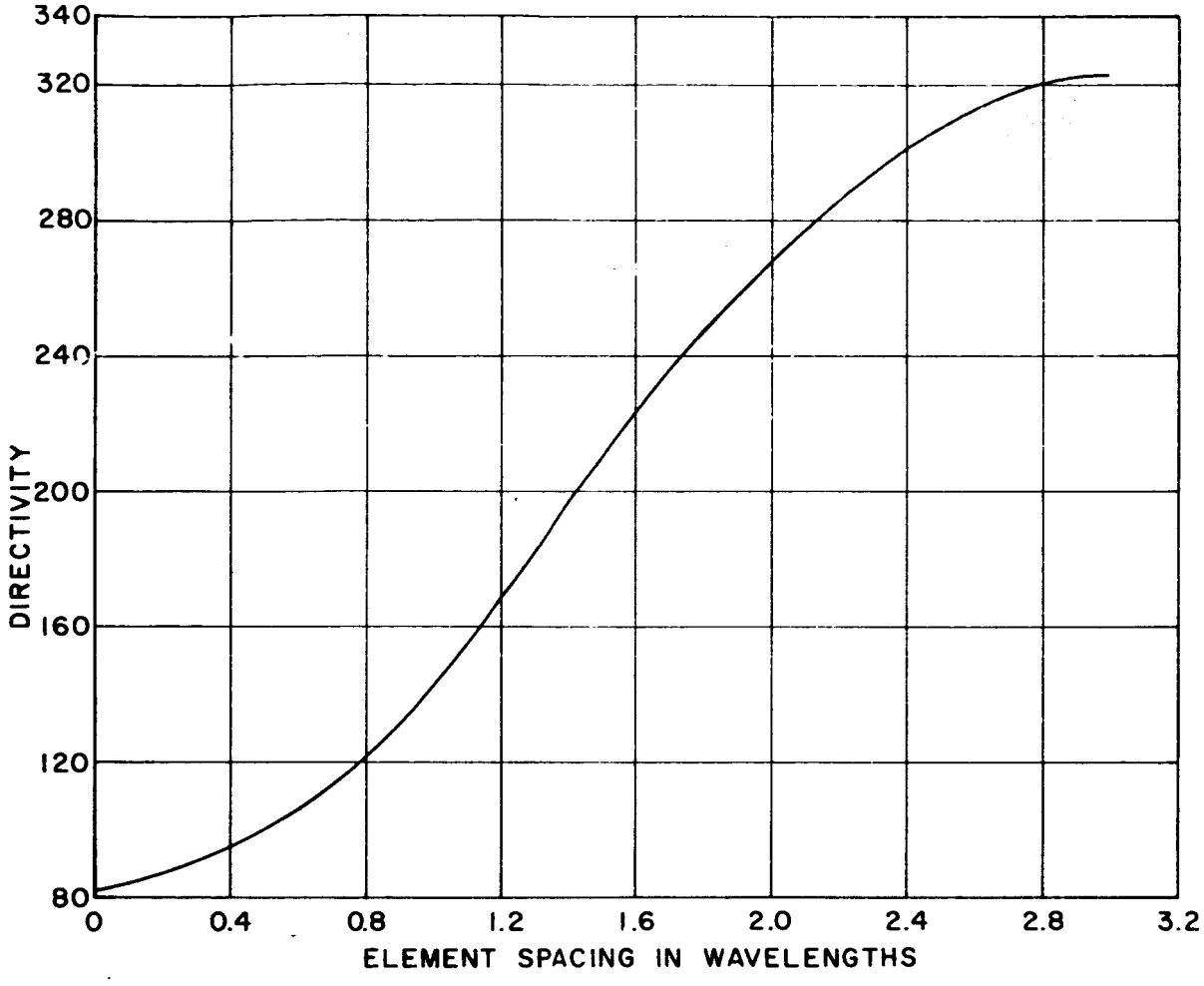

Fig. 12. Directivity of planar array of elements with $\cos^{20}\theta$ voltage pattern.

CHAPTER III
EXPERIMENTAL WORK

1. Introduction and Purpose

The accuracy of pattern multiplication is dependent, according to King[12], on whether the individual elements all have the same field pattern regardless of :

1. Their location in the array,
2. The relative amplitude and phase of the excitation,
3. The impedance of a generator or load connected across terminal pairs.

Stating it somewhat differently, Allen[13] says pattern multiplication is correct to the extent that the terminal conditions completely specify the currents flowing on the radiators. For the cases where this is not true and pattern multiplication does not apply, Hines et al.[14] suggest superposition of the patterns of each individual element with all other elements present but open-circuited. Allen[13, 15], working with thin half-wave dipoles, used pattern multiplication taking as the individual element pattern that pattern obtained with all other elements present but terminated in an effective generator impedance. Thus he assumes the current distribution on all elements to be identical and, for this reason, restricts his calculations to thin half-wave dipoles.

In the directivity calculations performed in Chapter II it was assumed that the $\cos^n\theta$ pattern of an individual element was unaffected by the presence of other array elements, thereby justifying the use of pattern multiplication.

It is the purpose of this chapter to show for what element spacings pattern multiplication, and consequently the calculated curves of Chapter II, is valid for the case of the four-element planar array. We will then observe for what element spacing the optimum pattern was obtained. Also in this chapter experimental patterns are presented which show, contrary to expectation, that although the radiation pattern of an individual element of this array becomes severely distorted for smaller spacings, pattern multiplication still produced a reasonably accurate pattern.

2. Description of the Four-Element Planar Array

The array (Figs. 13, 15) exhibits three-fold symmetry in the azimuthal plane, and for directive endfire elements, such as helices, the array pattern is relatively independent of the azimuthal angle. The helix (Fig. 13) was used for the individual element since it possessed the desired radiation characteristics, was believed to have low power coupling between elements, and could be supported mechanically so that the spacing between elements could be easily varied. To provide mechanical support the helices were wound on

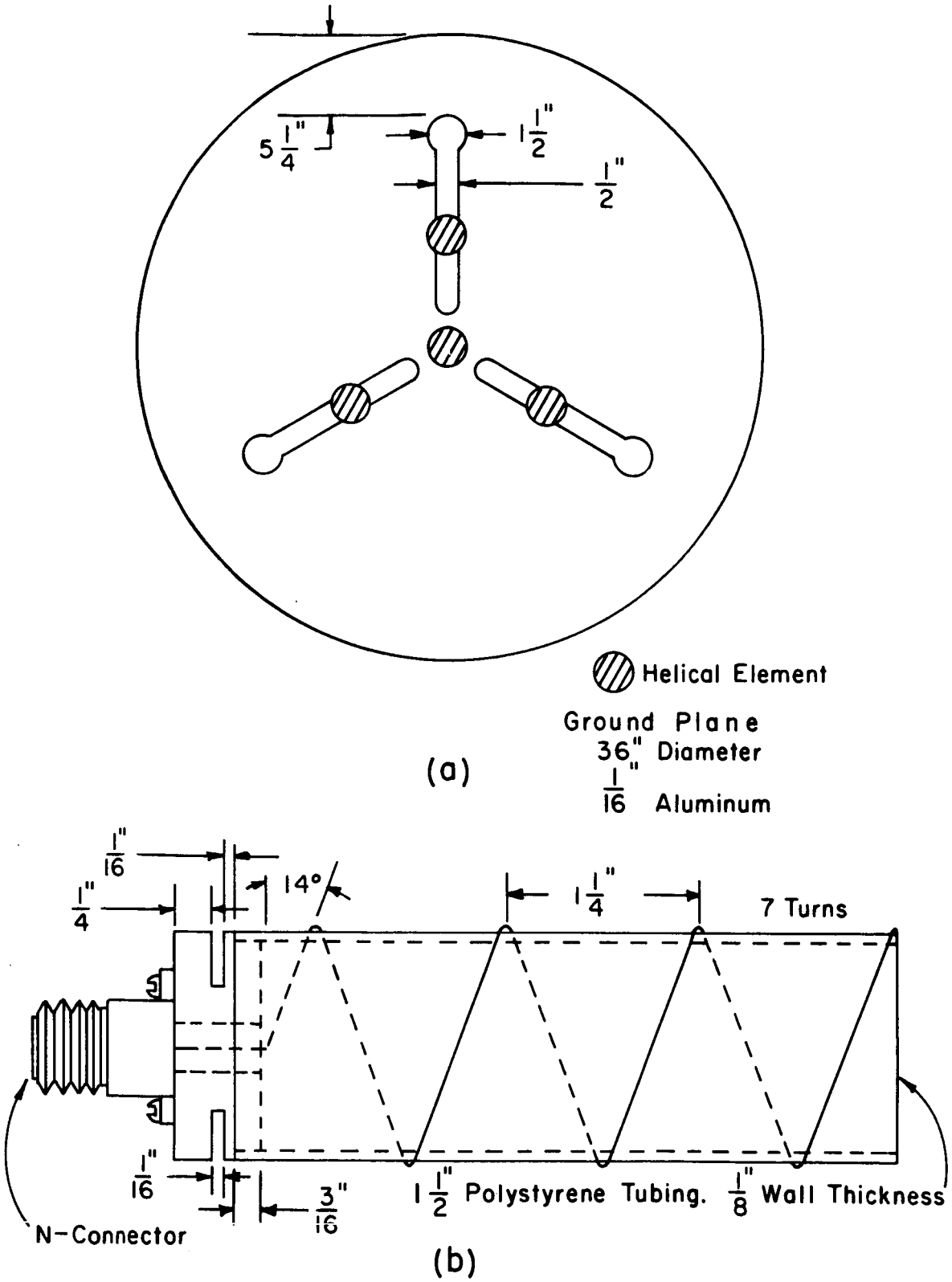

Fig. 13. Dimensions of planar array. (a) Ground plane with helical element, (b) Helical element.

$1\frac{1}{2}$-inch diameter polystyrene tubing. It was originally believed that the tubing would have little effect since Jones[16] and Hame[17] concluded that the main effect of winding a helix around a polystyrene rod is to shift the optimum operating frequency. This, however, was not found to be the case for the dimensions used here. The optimum operating frequency was not affected by the tubing, but the pattern (Fig. 14) is more directive than would be predicted by criteria presented by Kraus[18]. One explanation of the high directivity of the antenna is that the dielectric tube acts as a form of polyrod antenna. Such a dielectric tube can support a HE_{11} mode[19] which can be excited by a helix[20]. Radiation patterns obtained by Kelly[21] show a dielectric tube to be more directive than a helix of the same

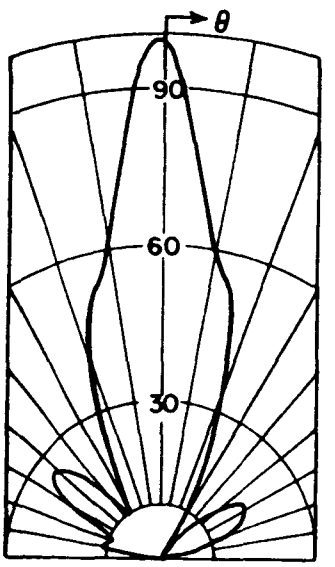

Fig. 14. Helix voltage pattern.

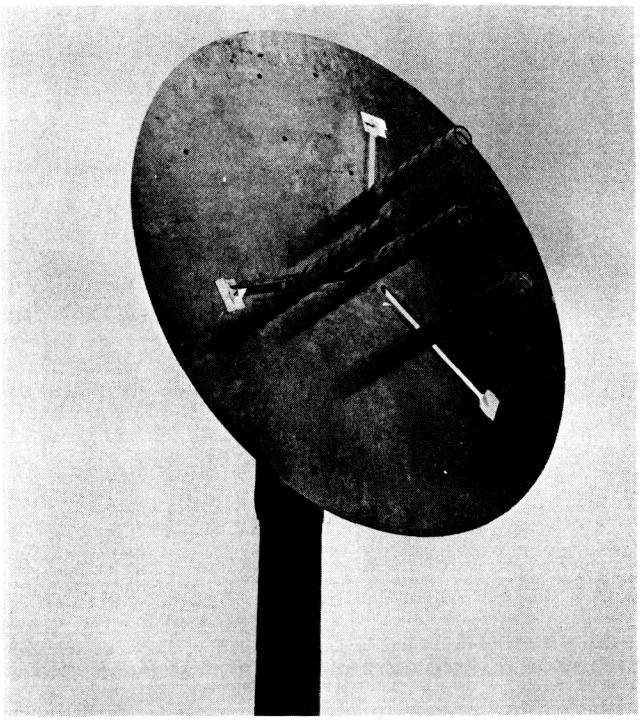

Fig. 15. Photograph of the array.

length. Also Kelly states there is significant radiation from the end of a dielectric tube when the length is less than two wavelengths[22]. This might be a cause of the distorted main lobe.

Other experimental observations made were:

1. The optimum operating frequency was 2500 mcs, corresponding to a helix circumference of one wavelength.
2. The directivity of a helix pattern was approximately equal to the directivity of a $\cos^n\theta$ pattern with $n = 10$.
3. The side lobe level increased from -14 db to -12 db as the helix was moved towards the edge of the ground plane.

4. The slots in the ground plane had negligible effect on the array pattern.

5. The patterns of the different helices were identical.

6. The element pattern became severely distorted for small element spacings. This effect will be discussed in a later section.

3. Experimental Results

The experimental patterns were taken with the four-element array acting as a receiving antenna (Fig. 15). The transmitting antenna was a parabolic reflector with a half-wave dipole feed. A small current probe was mounted on the ground plane near the feed of each helix to monitor the terminal current. A discussion of the probes and their response has been included as Appendix E. A diagram of the experimental set-up is shown in Fig. 16.

Experimental field patterns of the planar array are shown in Figs. 17-19 for element spacings corresponding to 5/6 through 13/6 wavelengths incremented by 1/6 wavelength steps. For a demonstration of the similarity of horizontally and vertically polarized patterns see Fig. 20. The preceding patterns were taken at an azimuth angle of 90° (Fig. 1). Patterns taken for other azimuth angles were consistent with those presented here.

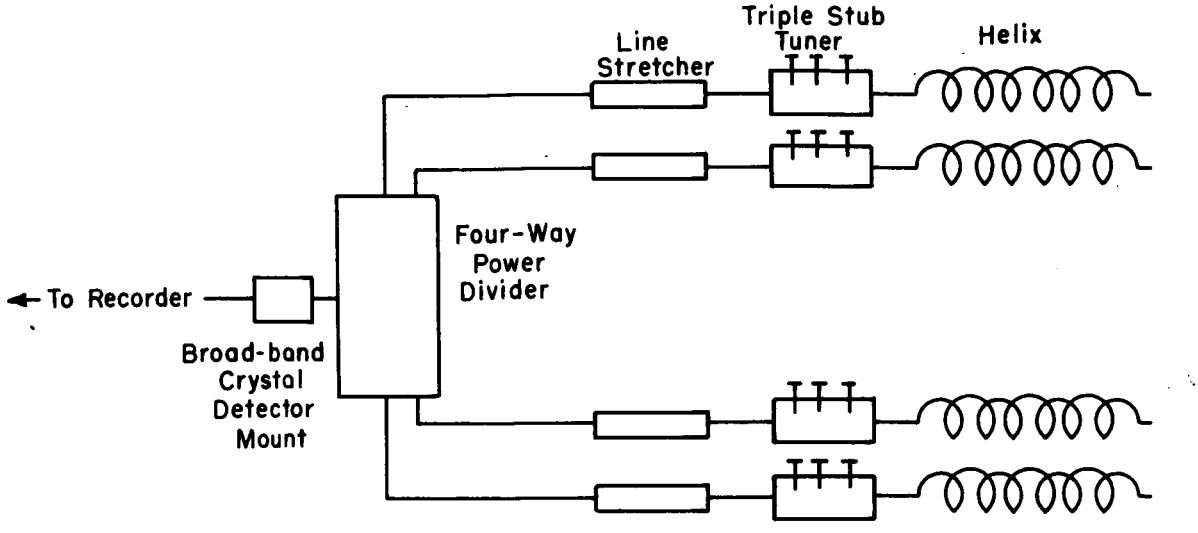

Fig. 16. Experimental setup.

The pattern of the planar array was calculated by pattern multiplication; the pattern of an isolated helix as shown in Fig. 14 being multiplied by the array factor. A comparison of the experimental array pattern and this calculated pattern is shown in Fig. 21 for element spacings of 13/6 and 9/6 wavelengths. The patterns are similar, with only minor discrepancies in the side lobe levels. The patterns of the individual elements become distorted for elements spacings of less than 5/4 wavelengths, with the center element the most distorted. To illustrate this, the center element

pattern is shown in Fig. 22 for three situations: as an isolated element, with the peripheral elements open-circuited, and with the peripheral elements short-circuited, the latter two situations corresponding to an element spacing of 5/6 wavelengths. The open circuit and short circuit conditions were determined by terminating each peripheral element with an adjustable short-circuited transmission line and varying the length of the line for maximum or minimum antenna terminal current as measured by the current probe response. From these patterns it is obvious that for the smaller spacings the basic assumption of pattern multiplication is violated since the terminal current no longer specifies the current distribution on the individual elements. A discussion of other terminal measurements has been included as Appendix F, where the isolation between elements and the performance of the current probes are discussed. The result of applying pattern multiplication with the isolated element pattern for a spacing of 5/6 wavelengths is shown in Fig. 23. A more accurate pattern has been obtained than could be anticipated in view of the distorted element patterns at this spacing.

In this section we have determined the array pattern by using the isolated element pattern which has a directivity of 40 (or 16 db). For larger spacings pattern multiplication worked well, with the best array pattern occurring for an element spacing of 2 wavelengths.

Smaller spacing resulted in an increased half-power beamwidth, while for larger spacings the number of side lobes increased. Consequently for this particular array we can conclude array multiplication is applicable for the spacings of interest - namely, those approximating the conditions for maximum directivity.

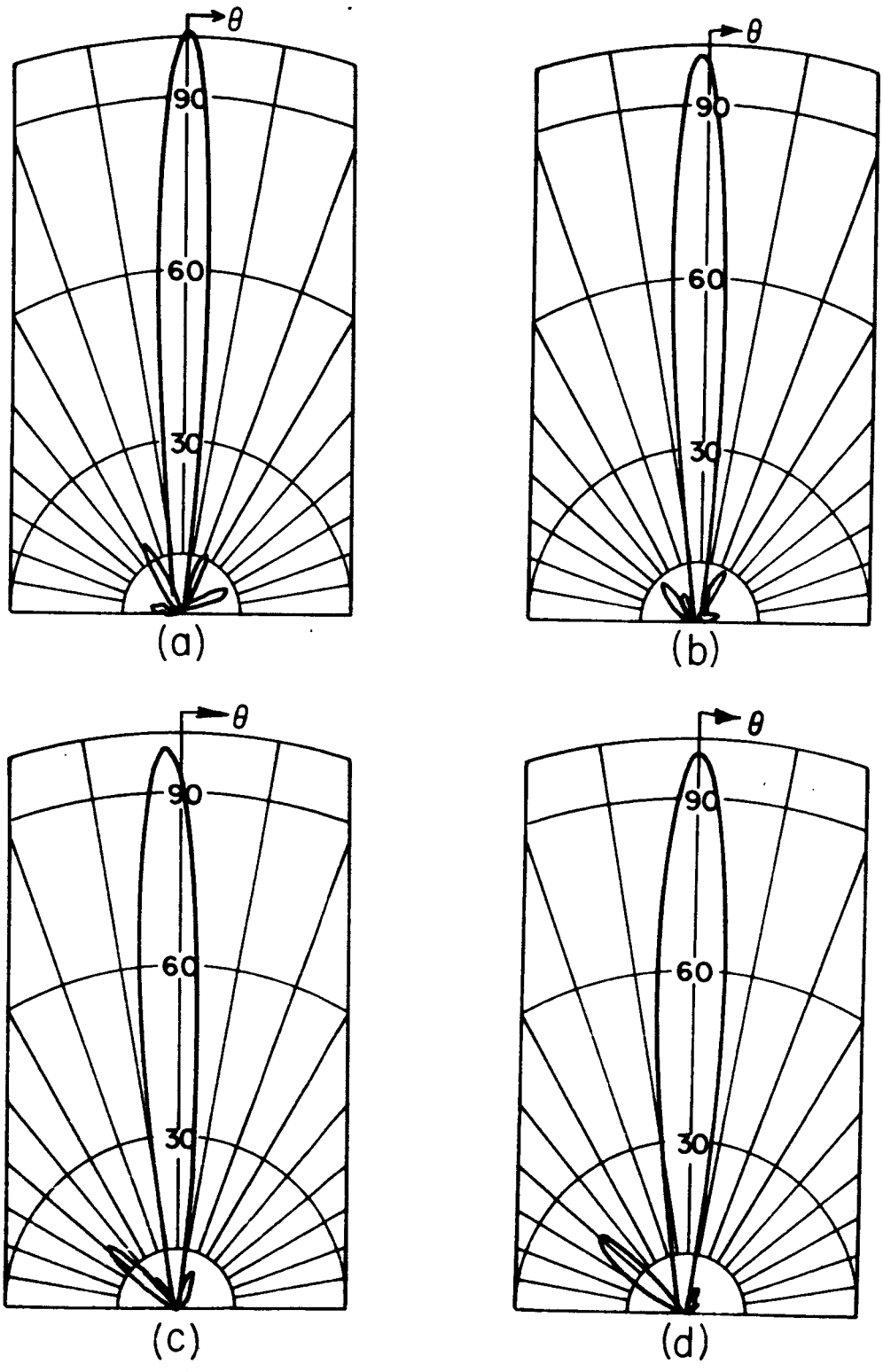

Fig. 17. Array voltage patterns with element spacings of (a) 13/6 wavelengths, (b) 12/6 wavelengths, (c) 11/6 wavelengths, (d) 10/6 wavelengths.

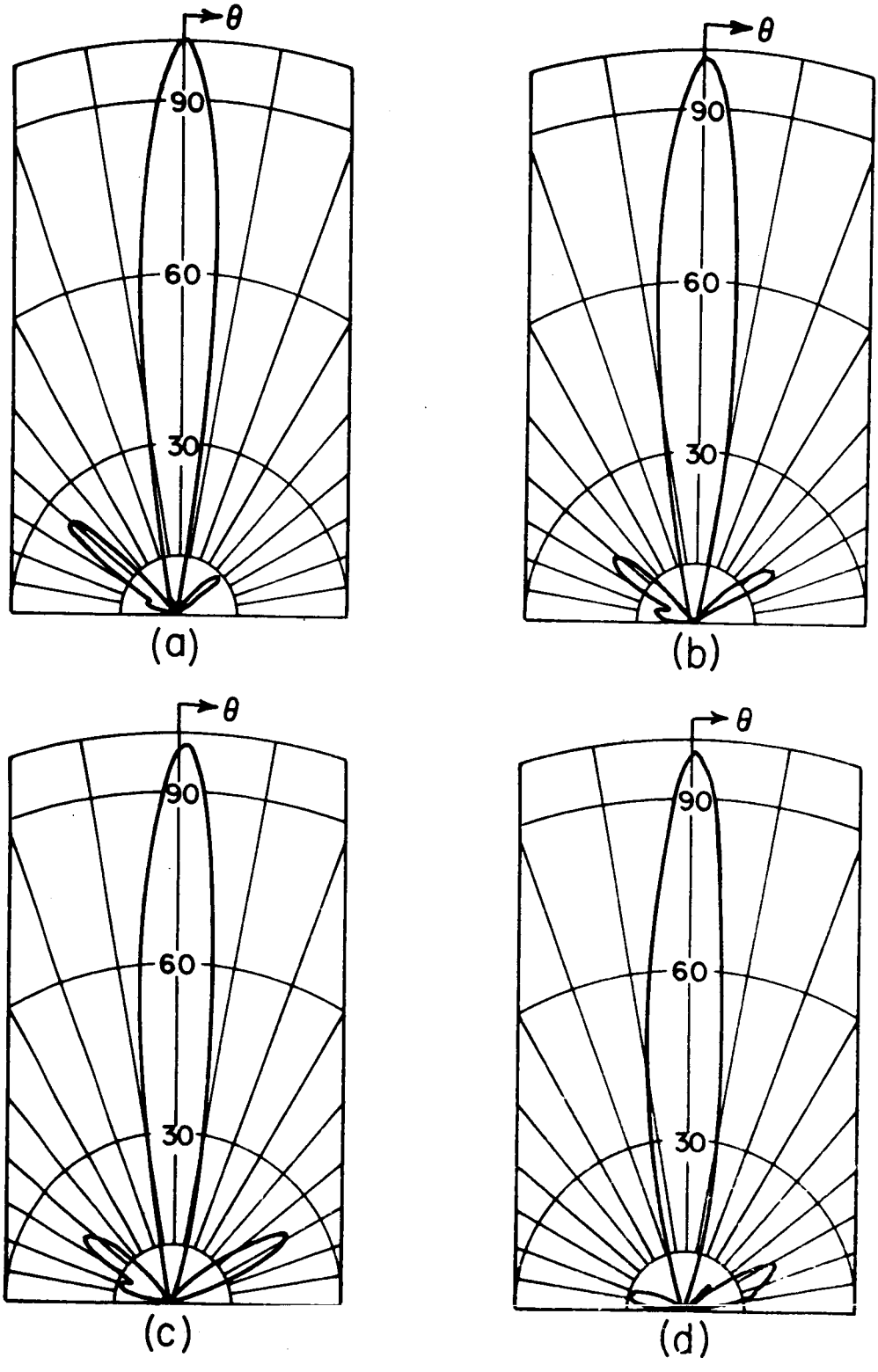

Fig. 18. Array voltage pattern with element spacing of (a) 9/6 wavelengths, (b) 8/6 wavelengths, (c) 7/6 wavelengths, (d) 6/6 wavelengths.

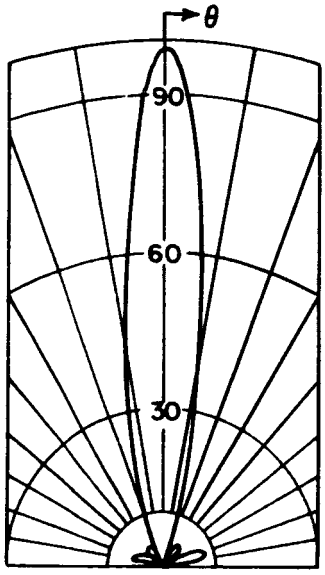

Fig. 19. Array voltage pattern with element spacing of 5/6 wavelengths.

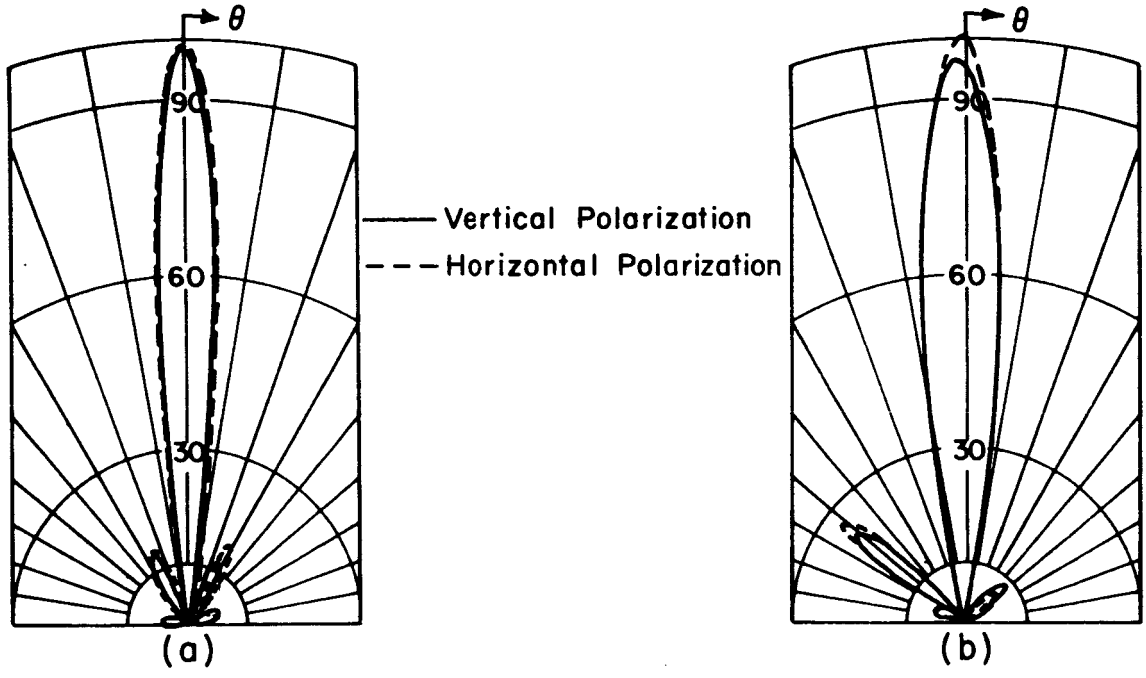

Fig. 20. Comparison of vertically polarized and horizontally polarized array voltage pattern for element spacings of (a) 13/6 wavelengths, (b) 9/6 wavelengths.

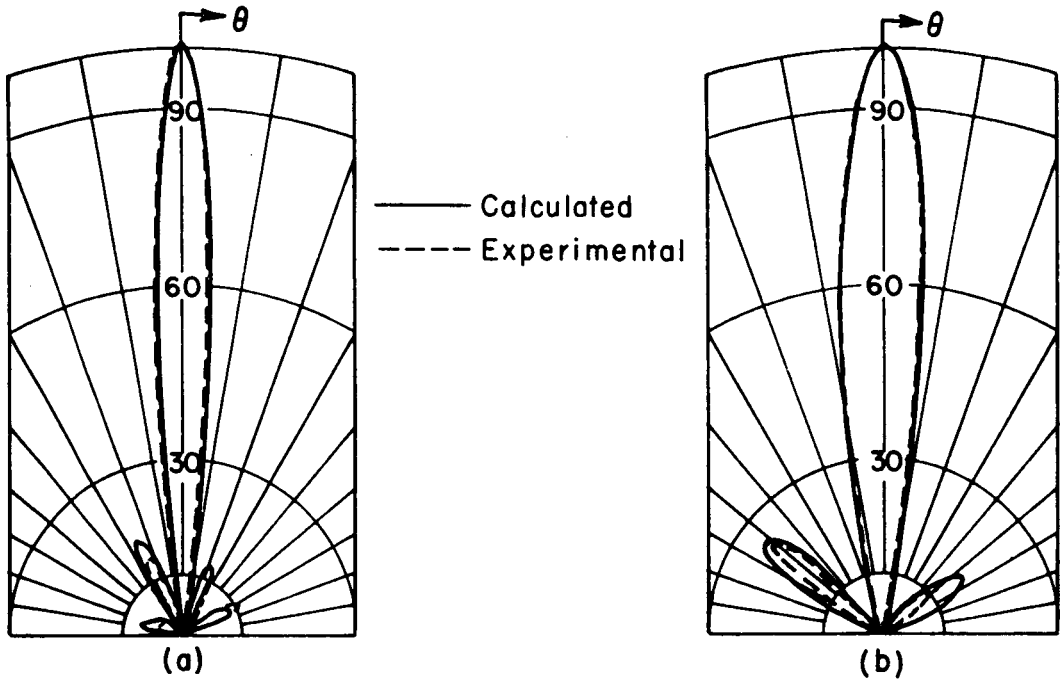

Fig. 21. Comparison of calculated and experinental array voltage patterns for element spacings of (a) 13/6 wavelength, (b) 9/6 wavelengths.

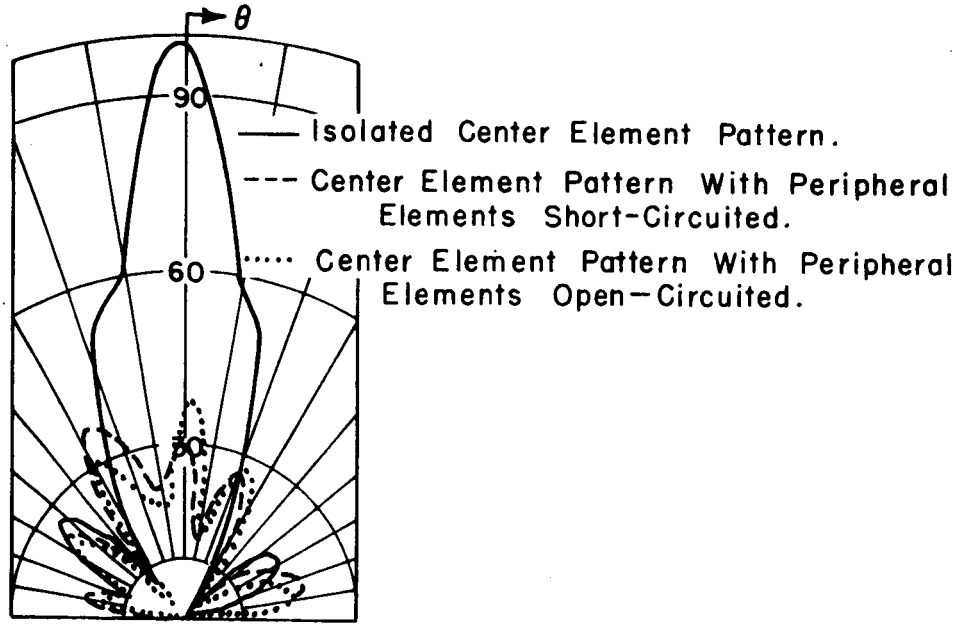

Fig. 22. Illustration of the effect of the peripheral elements on the voltage patterns of the center element at an element spacing of 5/6 wavelengths.

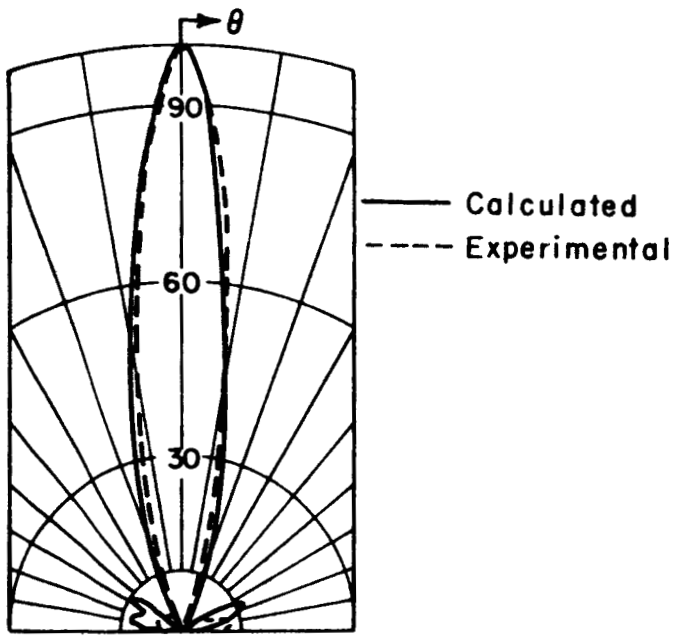

Fig. 23. Comparison of calculated and experimental array voltage patterns for an element spacing of 5/6 wavelengths.

CHAPTER IV
RESULTS AND CONCLUSIONS OF THE DIRECTIVITY CALCULATIONS

In this chapter the results of the directivity calculations of Chapter II will be used to assess the effective aperture concept as a criterion for determining an optimum spacing for directive elements.

The effective aperture A of an antenna is equal to the ratio of the power in the terminating impedance to the power density of the incident wave[23]. The effective aperture of a matched and lossless antenna can then be equated to the directivity D as[24]

$$A = \frac{\lambda^2}{4\pi} D \quad . \tag{3-1}$$

This definition, as has been pointed out by Tai[25], also assumes a polarization match between the incident field and the receiving antenna. If we take the aperture as the area of a circle then its diameter, measured in wavelengths, is

$$d_\lambda = \frac{\sqrt{D}}{\pi} \quad . \tag{3-2}$$

It has been conjectured that spacing the elements of a broadside array at element spacings of d_λ would be optimum. (Dr. Kraus had used the effective aperture concept in the design of his radio

telescope.[26, 27] To demonstrate that this is reasonable the following heuristic argument may be presented. Think of the effective aperture as an area which intercepts an incident wave. Each element of the array has this area which is related to the element directivity by (3-1). If the elements are spaced more distant than d_λ, the aperture of each antenna is not affected by the other apertures, resulting in a total array aperture of four times that of a single element (since we have four elements). This, from (3-1), produces an array directivity of four times that of an individual element. Now as the element spacing is decreased the effective apertures will overlap, thereby decreasing the total array aperture. Decreasing the distance to zero produces complete overlapping, resulting in a directivity equal to that of a single element. From this argument we conclude that the more directive the individual element, the larger should be the spacings where the effective apertures begin to overlap, consequently the larger must be the element spacing to achieve maximum directivity. This maximum directivity must be equal to the product of the number of elements and the directivity of a single element, and we shall call it D_∞. This definition does not take into consideration the situations where the directivity can exceed D_∞.

In addition to the comments made in Chapter II with regard to the directivity curves (Figs. 4-12) we observe the following.

1. The more directive the individual element, the larger must be the element spacing before D_∞ is attained. This is as predicted by the effective aperture concept.
2. For reasonably directive elements the directivity approaches D_∞ asymptotically. For a small sacrifice in directivity, the elements can be spaced somewhat more compactly.
3. Values of directivity exceeding D_∞ are achieved for only the less directive elements.

From the curves of Figs. 4-12, Table II has been prepared.

TABLE II
Summary of the Directivity Calculations

Individual Element Pattern	Directivity of Individual Element	D_∞	Element Spacing in Wavelengths In Accordance With the Aperture Concept $\frac{D}{\pi}$	Element Spacing in Wavelengths Where D_∞ First Attained	Directivity at $d_\lambda = \frac{\sqrt{D}}{\pi}$ D_A	$\frac{D_A}{D_\infty}$	$\frac{D_A}{D_\infty}$ in db
$\cos^0\theta$	2	8	.45	.41	9.5	1.19	0.74
$\cos^1\theta$	6	24	.78	.73	24.7	1.06	0.25
$\cos^2\theta$	10	40	1.00	.94	42.	1.05	0.21
$\cos^3\theta$	14	56	1.19	1.19	56	1.0	0.0
$\cos^4\theta$	18	72	1.35	1.32	72.	1.01	0.02
$\cos^8\theta$	34	136	1.85	2.08	134.	0.99	-0.04
$\cos^{12}\theta$	50	200	2.25	2.8	196.	0.98	-0.09
$\cos^{16}\theta$	66	264	2.59	3.4	258.	0.98	-0.09
$\cos^{20}\theta$	82	328	2.89	-	322.	0.98	-0.09

Of special significance is the last column which shows the ratio of the directivity of the array corresponding to $d_\lambda = \sqrt{D/\pi}$ and of D_∞. In other words this shows the difference in directivity between D_∞ and the directivity attained by spacing the elements according to the aperture concept.

As can be seen from Table II, the spacing of elements in the broadside planar array at a distance corresponding to the diameter of an individual element's effective aperture provides a good criterion for spacing the elements in order to attain the maximum directivity possible from the array. For more directive elements it may be desirable to space the elements somewhat closer than predicted from their apertures at a small sacrifice in directivity. Although it should be noted that for element spacing less than d_λ the directivity curves become approximately linear such that any decrease in element spacing has associated with it a decrease in directivity. For the less directive elements one may find it desirable to space the elements to benefit from the oscillatory behavior of the directivity. As a final note let us apply the aperture criterion to the experimental array. The individual elements had a directivity of approximately 40. Consequently we would want to space the elements at a distance equal to $\sqrt{40/\pi} = 1.98$ wavelengths. This was the spacing found to be optimum in the discussion of experimental results.

APPENDIX A
REDUCTION OF POWER EXPRESSION

Given the equation

$$(A\text{-}1) \qquad E(\theta,\phi)\,E(\theta,\phi)^* = \cos^{2n}\theta\left\{1 + 2\sum_{n=2}^{4}\cos(g\,\sin\theta\cos(\phi-\alpha_n)) + \sum_{n=2}^{4}\sum_{m=2}^{4} e^{jg\sin\theta(\cos(\phi-\alpha_m)-\cos(\phi-\alpha_n))}\right\},$$

and noting that $2\cos B = e^{jB} + e^{-jB}$ we can write

$$(A\text{-}2) \qquad E(\theta,\phi)\,E(\theta,\phi)^* = \cos^{2n}\theta\left\{4 + 2\sum_{n=2}^{4}\left[\cos(g\sin\theta\cos(\phi-\alpha_n))\right] + 2\cos[g\sin\theta(\cos(\phi-\alpha_3) - \cos(\phi-\alpha_2))] + 2\cos[g\sin\theta(\cos(\phi-\alpha_4) - \cos(\phi-\alpha_3))] + 2\cos[g\sin\theta(\cos(\phi-\alpha_4) - \cos(\phi-\alpha_2))]\right\}.$$

Observing that

$\cos(\phi-\alpha_m) - \cos(\phi-\alpha_n)$ equals

$[\cos\alpha_m - \cos\alpha_n]\cos\phi + [\sin\alpha_m - \sin\alpha_n]\sin\phi$

and making the substitutions $\alpha_2 = 180°$, $\alpha_3 = 300°$, $\alpha_4 = 60°$ Eq. (A-2) can be written as

$$(A\text{-}3) \qquad E(\theta,\phi)\,E(\theta,\phi)^* = \cos^{2n}\theta\left\{4 + 2\cos(g\sin\theta\cos\phi) \; 2\cos\left[g\sin\theta\left(\frac{1}{2}\cos\phi - \frac{\sqrt{3}}{2}\sin\phi\right)\right] \; 2\cos\left[g\sin\theta\left(\frac{1}{2}\cos\phi + \frac{\sqrt{3}}{2}\sin\phi\right)\right]\right.$$

(A-3) cont.

$$+ 2\cos\left[g\sin\theta\left(\frac{3}{2}\cos\phi - \frac{\sqrt{3}}{2}\sin\phi\right)\right]$$

$$+ 2\cos\left[\sqrt{3}g\sin\theta\sin\phi\right]$$

$$+ 2\cos\left[g\sin\theta\left(\frac{3}{2}\cos\phi + \frac{\sqrt{3}}{2}\sin\phi\right)\right]\Bigg\}.$$

Upon expanding the trigonometric functions in (A-3) and combining terms we finally have

(A-4)
$$E(\theta,\phi)\,E(\theta,\phi)^* = \cos^{2n}\theta\Bigg\{4 + 2\cos(g\sin\theta\cos\phi)$$

$$+ 4\cos\left(\frac{g}{2}\sin\theta\cos\phi\right)\cos\left(\frac{\sqrt{3}}{2}g\sin\theta\sin\phi\right)$$

$$+ 4\cos\left(\frac{g}{2}\sin\theta\cos\phi\right)\cos\left(\frac{\sqrt{3}}{2}g\sin\theta\sin\phi\right)$$

$$+ 2\cos(\sqrt{3}g\sin\theta\sin\phi)\Bigg\}.$$

APPENDIX B
INTEGRATION OF POWER EXPRESSION

In this appendix we will evaluate the expression

$$\text{(B-1)} \qquad \cos^{2n}\theta \int_0^{2\pi} \Big[4 + 2\cos(g \sin\theta \cos\phi) + 4\cos\Big(\frac{g}{2}\sin\theta\cos\phi\Big)\cos\Big(\frac{\sqrt{3}}{2} g \sin\theta\sin\phi\Big) + 4\cos\Big(\frac{3g}{2}\sin\theta\cos\phi\Big)\cos\Big(\frac{\sqrt{3}}{2} g \sin\theta\sin\phi\Big) + 2\cos(\sqrt{3}g \sin\theta\sin\phi)\Big] d\phi \,.$$

Taking the identities [28]

$$\text{(B-2)} \qquad \cos(x \sin\phi) = J_o(x) + 2\sum_{k=1}^{\infty} J_{2k}(x)\cos 2k\phi \,,$$

$$\text{(B-3)} \qquad \sin(x \sin\phi) = 2\sum_{k=1}^{\infty} J_{2k-1}(x)\sin(2k-1)\phi,$$

$J_n(x)$ being the n^{th} order Bessel function of the first kind, and integrating each side from $\phi = \alpha$ to $\phi = 2\pi + \alpha$, α being any real constant, we obtain

$$\text{(B-4)} \qquad J_o(x) = \frac{1}{2\pi}\int_{\alpha}^{2\pi+\alpha} \cos(x \sin\phi)\, d\phi \,,$$

$$\text{(B-5)} \qquad 0 = \int_{\alpha}^{2\pi+\alpha} \sin(x \sin\phi)\, d\phi \,.$$

Replacing the integral of the sum by the sum of the integrals in (B-1), two integrations are now immediate; namely,

$$\text{(B-6)} \qquad \int_0^{2\pi} 4\, d\phi = 8\pi$$

and

$$\text{(B-7)} \qquad 2\int_0^{2\pi} \cos(\sqrt{3}g \sin\theta \sin\phi)d\phi = 4\pi J_0(\sqrt{3}g).$$

The following integration,

$$2\int_0^{2\pi} \cos(g \sin\theta \cos\phi)d\phi,$$

is also immediate from (B-4) upon the substitution $\phi = \eta - 90°$ yielding

$$\text{(B-8)} \qquad 2\int_0^{2\pi} \cos(g \sin\theta \cos\phi)d\phi = 4\pi J_0(g \sin\theta).$$

In (B-1) we have two integrals left to evaluate.

We consider first the integral

$$\text{(B-9)} \qquad 4\int_0^{2\pi} \cos\left(\frac{g}{2} \sin\theta \cos\phi\right)\cos\left(\frac{\sqrt{3}}{2} g \sin\theta \sin\phi\right)d\phi$$

which upon utilizing the identity $\cos A \cos B = \frac{1}{2}\cos(A-B) + \frac{1}{2}\cos(A+B)$ becomes

$$\text{(B-10)} \qquad 2\int_0^{2\pi} \cos\left(g \sin\theta\left(\frac{1}{2}\cos\phi - \frac{3}{2}\sin\phi\right)\right)d\phi +$$

$$2\int_0^{2\pi} \cos\left(g \sin\theta\left(\frac{1}{2}\cos\phi + \frac{3}{2}\sin\phi\right)\right)d\phi$$

which equals

$$(B\text{-}11) \qquad 2\int_0^{2\pi} \cos(g \sin\theta \sin(\phi-30))\, d\phi + 2\int_0^{2\pi} \cos(g \sin\theta \sin(\phi+30))\, d\phi .$$

Upon substituting $\eta = \phi-30$ in the first integral and $\eta = \phi + 30$ in the second integral, (B-11) is of the form (B-4), consequently (B-9) becomes equal to $8\pi J_o(g \sin\theta)$.

In a similar manner the final integral to be evaluated is

$$(B\text{-}12) \qquad 4\int_0^{2\pi} \cos\left(\frac{3g}{2} \sin\theta \cos\phi\right)\cos\left(\frac{\sqrt{3}g}{2} \sin\theta \sin\phi\right)d\phi = 8\pi J_o(\sqrt{3} \sin\theta).$$

Combining the results of the integrations leading to (B-6), (B-7), (B-11), (B-12) we have (B-1) equal to

$$(B\text{-}13) \qquad \cos^{2n}\theta[8\pi + 12\pi J_o(g \sin\theta) + 12\pi J_o(\sqrt{3}g \sin\theta)] = 2\pi[4 + 6J_o(g \sin\theta) + 6J_o(\sqrt{3}g \sin\theta)]\cos^{2n}\theta .$$

APPENDIX C
INFINITE SERIES SOLUTION FOR DIRECTIVITY

In this section we will obtain an infinite-series solution to the integral

$$\text{(C-1)} \qquad \int_o^{\pi/2} [J_o(g \sin\theta) \cos^{2n}\theta \sin\theta]d\theta .$$

Making the substitution, $\beta = g \sin\theta$, (C-1) becomes

$$\text{(C-2)} \qquad \frac{1}{g^2} \int_o^g \left\{ \left[1 - \left(\frac{\beta}{g}\right)^2 \right]^{\frac{2n-1}{2}} \beta J_o(\beta) \right\} d\beta$$

whereupon by integration by parts we obtain

$$\text{(C-3)} \qquad \frac{1}{2n+1} \left[1 - \int_o^g \left\{ \left(1 - \frac{\beta^2}{g^2} \right)^{\frac{2n+1}{2}} J_1(\beta) \right\} d\beta \right] .$$

We now resubstitute the trigonometric functions by letting $\beta = g \sin\theta$ and (C-3) becomes

$$\text{(C-4)} \qquad \frac{1}{2n+1} \left[1 - g \int_o^{\pi/2} \left[\cos^{2n+2}\theta \, J_1(g \sin\theta) \right] d\theta \right] .$$

We now concentrate on the integral

$$\text{(C-5)} \qquad \int_o^{\pi/2} \cos^{2n+2}\theta \, J_1(g \sin\theta) d\theta$$

which, upon expanding the Bessel function, becomes

$$\int_0^{\pi/2} \left\{ \cos^{2n+2}\theta \sum_{m=0}^{\infty} \left[\frac{(-1)^m}{m!(m+1)!} \left(\frac{g}{2}\right)^{2m+1} \sin^{2m+1}\theta \right] \right\} d\theta . \tag{C-6}$$

Since in an uniformly convergent series we can interchange summation and integration we have

$$\sum_{m=0}^{\infty} \left[\frac{(-1)^m}{m!(m+1)!} \frac{g^{2m+1}}{2^{2m+1}} \int_0^{\pi/2} (\cos^{2n+2}\theta \sin^{2m+1}\theta) d\theta \right] \tag{C-7}$$

and our problem has simplified to the evaluation of

$$\int_0^{\pi/2} \cos^{2n+2}\theta \sin^{2m+1}\theta \, d\theta . \tag{C-8}$$

We note in particular that the index on the cosine function is an even integer and that the index on the sine function is an odd integer. We digress now and consider the integral

$$\int_0^{\pi/2} \cos^n x \sin^m x \, dx \tag{C-9}$$

where n is an even integer and m is an odd integer. Upon integrating (C-9) we obtain

$$\int_0^{\pi/2} \sin^m x \cos^n x \, dx$$

equals

$$\frac{-\sin^{m-1}x \cos^{n+1}x}{m+1} \Bigg|_0^{\pi/2} + \frac{m-1}{m+n} \int_0^{\pi/2} \sin^{m-2}x \cos^n x \, dx. \tag{C-10}$$

From consideration of (C-10) we can make the following observations. Because of the range of integration (0 to $\pi/2$) the first term on the right side of (C-10) is zero and the index on the sine function has decreased by 2 in the integrand. By mathematical induction we can write

$$(C\text{-}11) \qquad \int_o^{\pi/2} \sin^m x \cos^n x \, dx = \left[\frac{m-1}{m+n} \cdot \frac{m-3}{m+n-2} \cdot \frac{m-5}{m+n-4} \cdots \frac{2}{n+3}\right] \frac{1}{n+1} \, .$$

Letting $n = 2n + 2$ and $m = 2m+1$ in (C-11) we obtain for (C-8) that

$$C\text{-}12) \qquad \int_o^{\pi/2} \cos^{2n+2}\theta \sin^{2m+1}\theta \, d\theta = \left[\frac{2m}{2m+2n+3} \cdot \frac{2m-2}{2m+2n+1} \cdot \frac{2m-4}{2m+2n-1} \cdots \frac{2}{2n+5}\right] \frac{1}{2n+3} \, .$$

As can be seen in (C-12) the condition $m = 0$ is not applicable and must be considered separately. Doing this we have

$$(C\text{-}13) \qquad \int_o^{\pi/2} \sin\theta \cos^{2n+2}\theta = \frac{1}{2n+3} \, .$$

Now substituting (C-12) and (C-13) into (C-7) and finally substituting into (C-4) we have

$$(C\text{-}14)\qquad \int_0^{\pi/2} [J_0(g \sin\theta) \sin\theta \cos^{2n}\theta]\,d\theta =$$

$$\frac{1}{2n+1}\left[1 - \frac{g^2}{2(2n+3)} - g \sum_{n=1}^{\infty}\left\{\frac{(-1)^m}{m!(m+1)!}\ \frac{g^{2m+1}}{2^{2m+1}}\left(\frac{2m}{2m+2n+3}\cdot \frac{2m-2}{2m+2n+1} \cdots \frac{2}{2n+5}\right)\frac{1}{2n+3}\right\}\right].$$

To provide a check on this equation, one can observe that when $n = 0$ we have [29]

$$\int_0^{\pi/2} J_0(g \sin\theta) \sin\theta\, d\theta = \frac{\sin g}{g}$$

and that the right side of (C-14) does reduce to $\frac{\sin g}{g}$.

Define the right side of (C-14) to equal $S(g, n)$ then the expression obtained for directivity in Chapter II becomes

$$(C\text{-}15)\qquad D = \frac{16}{\frac{2}{2n+1} + S(g, n) + S(\sqrt{3}g, n)}\ .$$

The usefulness of Eq. (C-14) is limited by the value of g. If g becomes too large, the series converges slowly while the size of the terms in the series becomes very large. For values of g greater than six it would be advantageous to use other means for evaluating the integral expression (C-1).

APPENDIX D
COMPUTER PROGRAM DESCRIPTION

The flow sheet of the computer program is shown in Table III. Also included in this Appendix is a printout of the Scatran program used. More statements are included in the program than are actually needed since it was originally written for the more general case of unequal current excitations of the individual elements. A portion of the result printout is shown for the cases where n = 1, 2, and 3. The last page contains the data input which is the weights and sample points used in the Gaussian Quadrature formula.

TABLE III

Flow Diagram for the Computer Program

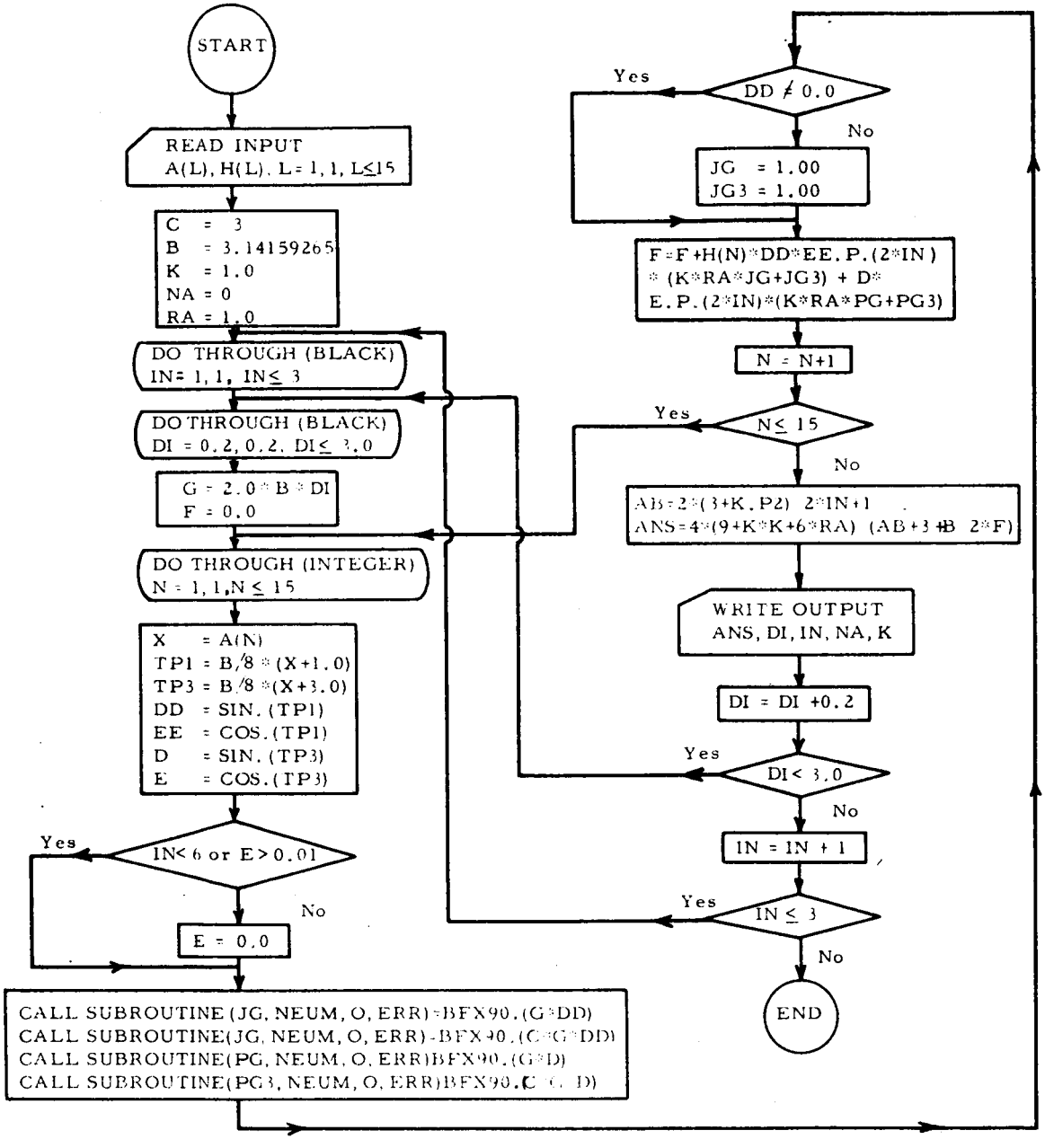

TABLE IV
Scatran Program Statements

```
PROGRAM STATEMENTS FOR DIRECTIVITY CALCULATIONS.

                DIMENSION (A(16),H(16))-                                    0000
                FLOATING (JG,JG3,K)-                                        0001
  START         READ INPUT ,GO,((A(L),H(L),L=1,1,L,LE,15))-                 0002
F GO            (2F12.8)     -                                              0003
                C=3.E.0.5-                                                  0004
                B=3.14159265-                                               0005
                C1=0.0-                                                     0006
  RED           C2=6.0-                                                     0007
  ORANGE        K=C1/C2-                                                    0008
                K=1.0-                                                      0009
                NA=0-                                                       0010
                RA=1.0-                                                     0011
                 DO THROUGH (BLACK),IN=1,1, PROVIDED (IN.LE.3)-             0012
                 DO THROUGH (BLACK),DI=0.2,0.2, PROVIDED (DI.LE.3.0)-       0013
                G=2.0*B*DI-                                                 0014
                F=0.0-                                                      0015
                 DO THROUGH (INTEGR),N=1,1, PROVIDED (N.LE.15)-             0016
                X=A(N)-                                                     0017
                TP1=B/8.0*(X+1.0)-                                          0018
                TP3=B/8.0*(X+3.0)-                                          0019
                DD=SIN.(TP1)-                                               0020
                EE=COS.(TP1)-                                               0021
                D=SIN.(TP3)-                                                0022
                E=COS.(TP3)-                                                0023
                 TRANSFER TO (BETA) PROVIDED (IN.LE.6.OR.E.G.0.01)-         0024
                E=0.00-                                                     0025
  BETA           CALL SUBROUTINE (JG,NEUM.0,ERR)=BFX90.(G*DD)-              0026
                 CALL SUBROUTINE (JG3,NEUM.0,ERR)=BFX90.(G*3*DD)-           0027
                 CALL SUBROUTINE (PG,NEUM.0,ERR)=BFX90.(G*D)-               0028
                 CALL SUBROUTINE (PG3,NEUM.0,ERR)=BFX90.(G*G*D)-            0029
                 TRANSFER TO (INTEGR) PROVIDED (D.NE.0.00)-                 0030
                JG=1.00-                                                    0031
                JG3=1.00-                                                   0032
  INTEGR        F=F+H(N)*(D)*EE.P.(2*IN)*(K*RA*JG+D3)+D*E.P.(2*IN)*(K*RA*P  0033
               G+PG3))-                                                     0034
                AB=2*(3+K.P.2)/(2*IN+1)-                                    0035
                ANS=4*(9+K*(K+6*RA))/(AB*3*RA**2)-                          0036
                 WRITE OUTPUT ,HOPE,(ANS,,I=1N,NA,K)-                       0037
  BLACK          CONTINUE -                                                 0038
                 TRANSFER TO (END)-                                         0039
                 TRANSFER TO (YELLOW) PROVIDED (C1.GE.6.0)-                 0040
                C1=C1+3.0-                                                  0041
                 TRANSFER TO (RED)-                                         0042
  YELLOW        C1=C1+6.0-                                                  0043
                 TRANSFER TO (ORANGE) PROVIDED (C1.LE.18.0)-                0044
F HOPE          (2F10.3,216,F10.4)-                                         0045
  END           CALL SUBROUTINE ()=ENDJOB.()-                               0046
                END PROGRAM (START)-                                        0047
```

TABLE V

Portion of Scatran Program Printout

Directivity	Element Spacing in Wavelengths	n
7.557	0.200	1
13.518	0.400	1
21.653	0.600	1
24.988	0.800	1
27.063	1.000	1
24.916	1.200	1
22.456	1.400	1
23.288	1.600	1
24.542	1.800	1
24.468	2.000	1
24.215	2.200	1
23.684	2.400	1
23.561	2.600	1
24.200	2.800	1
24.339	3.000	1
11.790	0.200	2
18.081	0.400	2
28.354	0.600	2
36.261	0.800	2
41.062	1.000	2
42.575	1.200	2
40.457	1.400	2
39.137	1.600	2
39.571	1.800	2
40.116	2.000	2
40.286	2.200	2
40.156	2.400	2
39.845	2.600	2
39.830	2.800	2
40.047	3.000	2
15.917	0.200	3
22.377	0.400	3
33.487	0.600	3
44.630	0.800	3
52.455	1.000	3
57.200	1.200	3
57.751	1.400	3
56.256	1.600	3
55.560	1.800	3
55.721	2.000	3
56.014	2.200	3
56.162	2.400	3
56.082	2.600	3
55.936	2.800	3
55.932	3.000	3

TABLE VI

Data Input

Sample Points	Weights
*** Data	
-0.98799251	0.03075324
-0.93727339	0.07036604
-0.84820658	0.10715922
-0.72441773	0.13957067
-0.57097217	0.16626920
-0.39415134	0.18616100
-0.20119409	0.19843148
0.00000000	0.20257824
0.20119409	0.19843148
0.39415134	0.18616100
0.57097217	0.16626920
0.72441773	0.13957067
0.84820658	0.10715922
0.93727339	0.07036604
0.98799251	0.03075324

APPENDIX E
DESCRIPTION OF THE CURRENT PROBES

In order to insure the array was uniformly excited at all element spacings, it was desirable to devise a method to detect any significant change in the element terminal currents. Current probes consisting of small shielded image loops were constructed and mounted on the ground plane, one near the feed of each helix as shown in Fig. 24. Assuming the probe was symmetrical and

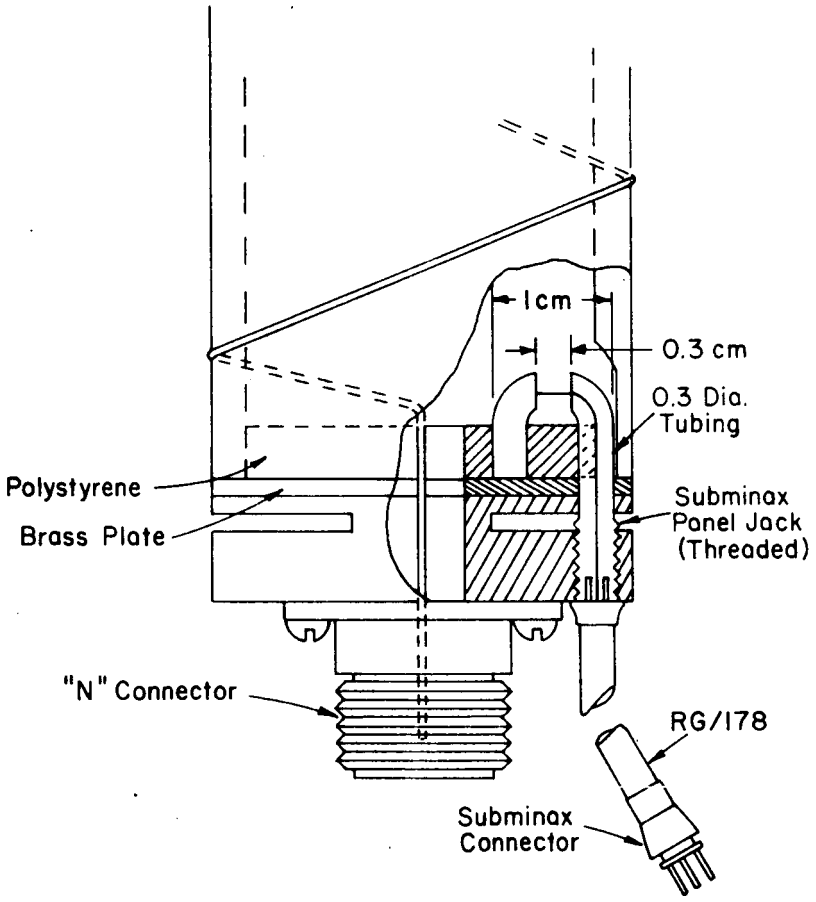

Fig. 24. Current probe.

sufficiently small, it would respond to only a magnetic field component. Then assuming a TEM mode exists, this component is proportional to the terminal current (because the space distribution is fixed).

The probe position relative to each helix is shown in Fig. 25.

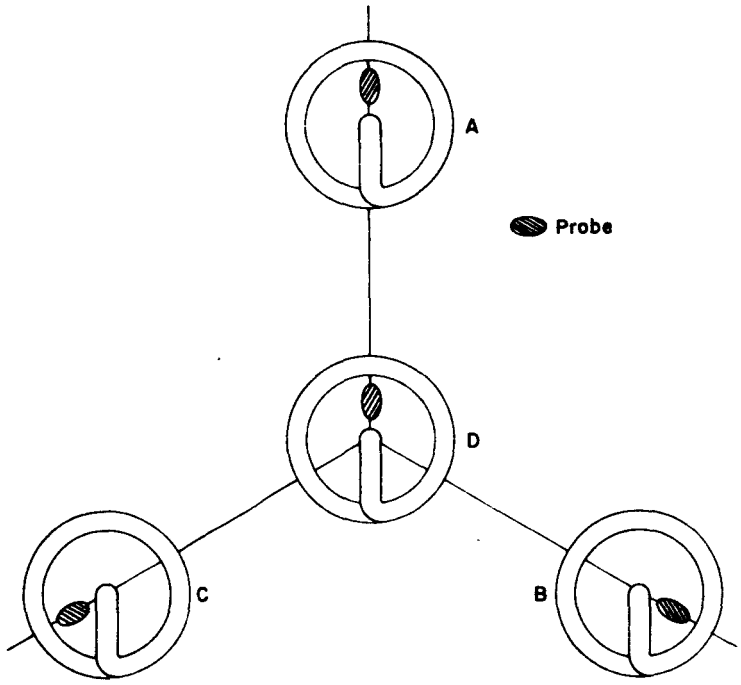

Fig. 25. Orientation of probes.

The probes have been designated by letters so that special attention might be called to a specific probe as these probes will again be referred to in Appendix F.

It was necessary to determine whether each probe was actually responding to the feed current of its helix alone. Methods shown by Whiteside[30] for separating the response due to the magnetic field

from the response of an electric field were not applicable to the experimental set-up. The methods that were used to ascertain the probe response and their results were:

1. Attenuation of an individual helix excitation resulted in an equal attenuation of the response of its probe.
2. Variation of the phase of an individual helix excitation resulted in a similar variation of the response of its probe.
3. Comparison of a helix pattern with the pattern of its probe, with the helix terminated in a matched load, resulted in agreement for probes A, B, and D. A typical pattern is shown in Fig. 26. The pattern of helix C was essentially not similar to its helix pattern and it was concluded the probe was not operating properly.

The above results were obtained only when the element spacing was sufficiently large, i.e., on the order of a wavelength.

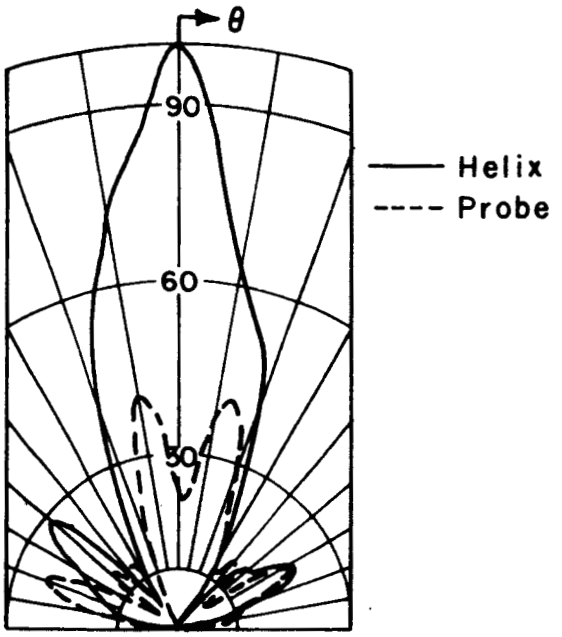

Fig. 26. Voltage pattern of a helix and its probe.

APPENDIX F
TERMINAL MEASUREMENTS

In this section we will present the results of measurements with the current probes and the results of measurements of power coupling between two helices as measured at their terminals.

The probes were used to monitor any change in the amplitude and relative phase of the excitation of each helix as the element spacing was varied. The results of these measurements are plotted in Fig. 27 and Fig. 28. Both plots have reference relative to an element spacing of 26 centimeters or 13/6 wavelengths. In order to achieve this small variation for the smaller element spacings a small conducting strip of aluminum was fastened to the polystyrene tubing opposite the probe of each antenna (see Fig. 29). Without this strip the variation in phase was as much as 21°.

A brief study was made of the power coupled to the terminals of one helix from another helix. If one considers two helices as shown in Fig. 30, the power coupling is dependent on the spacing between elements, the angle α, and the angle β. A plot of such coupling is shown in Fig. 31, where the angle β has been varied throughout 360° with the angle α fixed. Although there is a sharp minimum in coupled power, no conclusion could be made as to a relationship between any arbitrary angle α and the angle for which

a minimum occurred with the limited amount of experimental work performed. For the situation plotted in Fig. 31 a minimum occurred for $\alpha=\beta$ but this was not the case for other values of α.

Measurements were also made of the power coupled from the three peripheral elements of the four-element planar array to the center element. The results are shown in Fig. 32. From these measurements one could conclude that the mutual impedance between the helices is not a negligible quantity, even though traveling-wave structures of this type are often assumed to have very small mutual impedance.

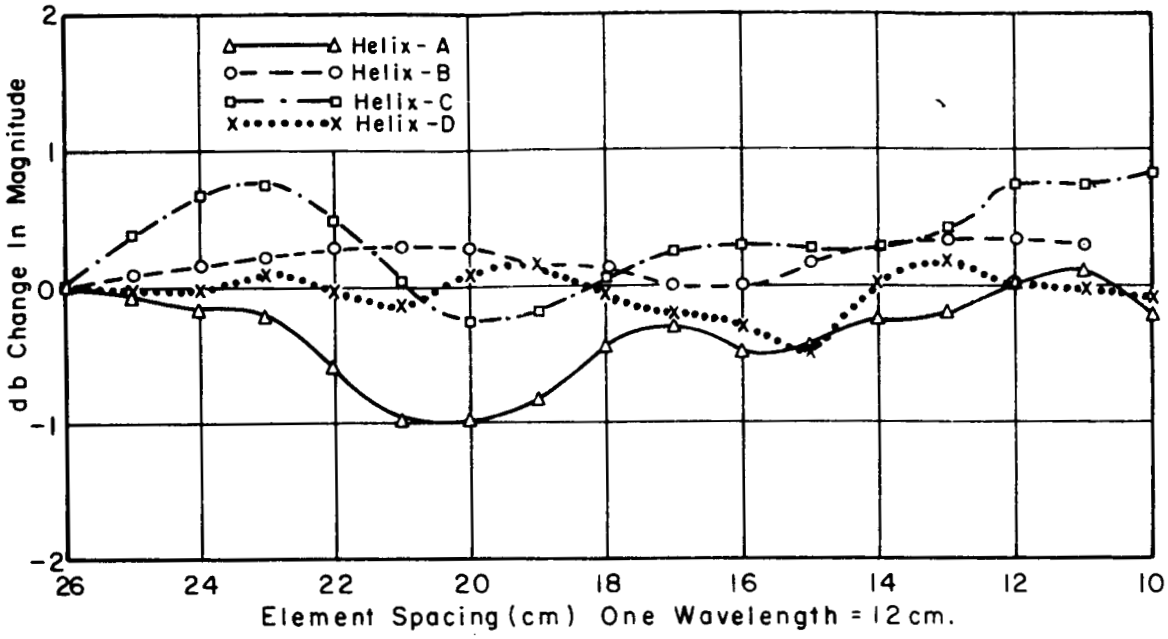

Fig. 27. Variation of probe signal with element spacing.

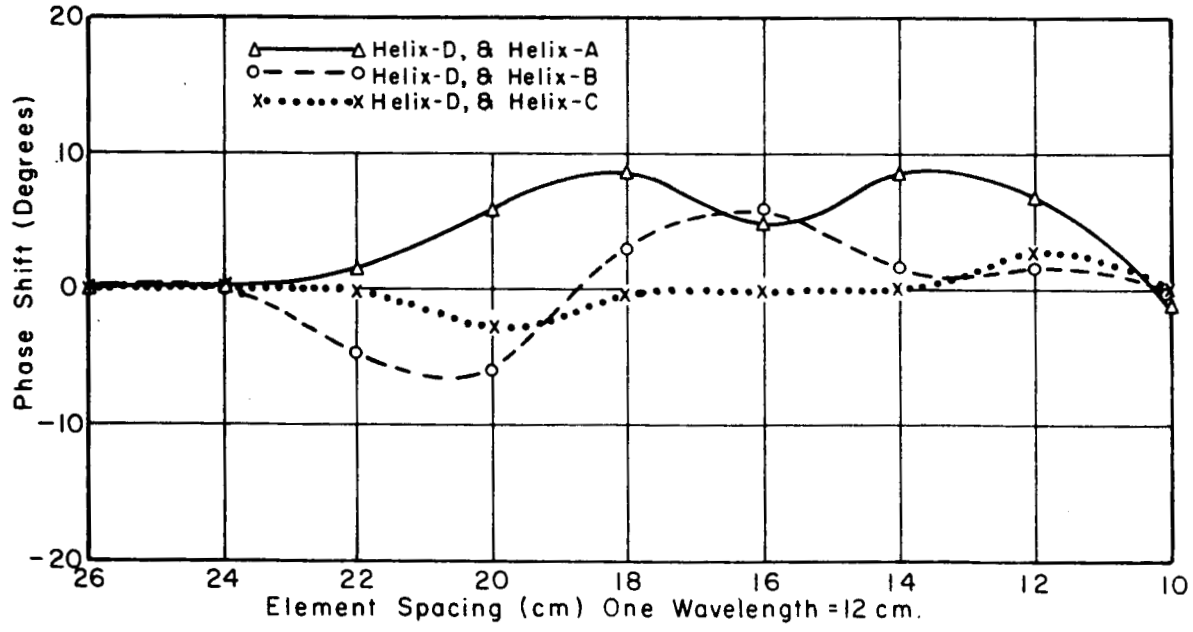

Fig. 28. Variation of phase between the middle element and the peripheral elements with element spacing.

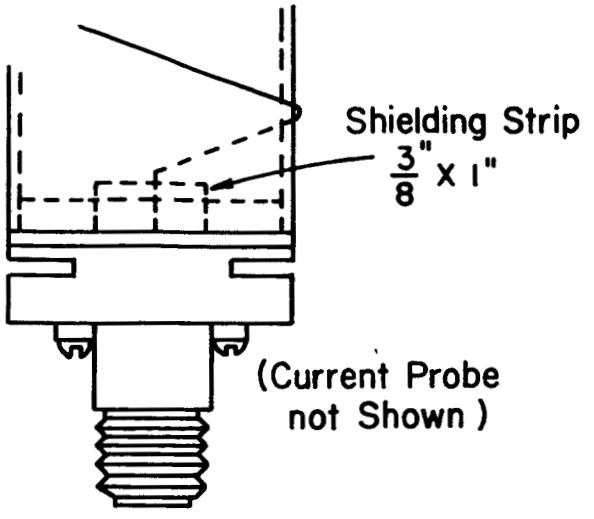

Fig. 29. Shielding strip.

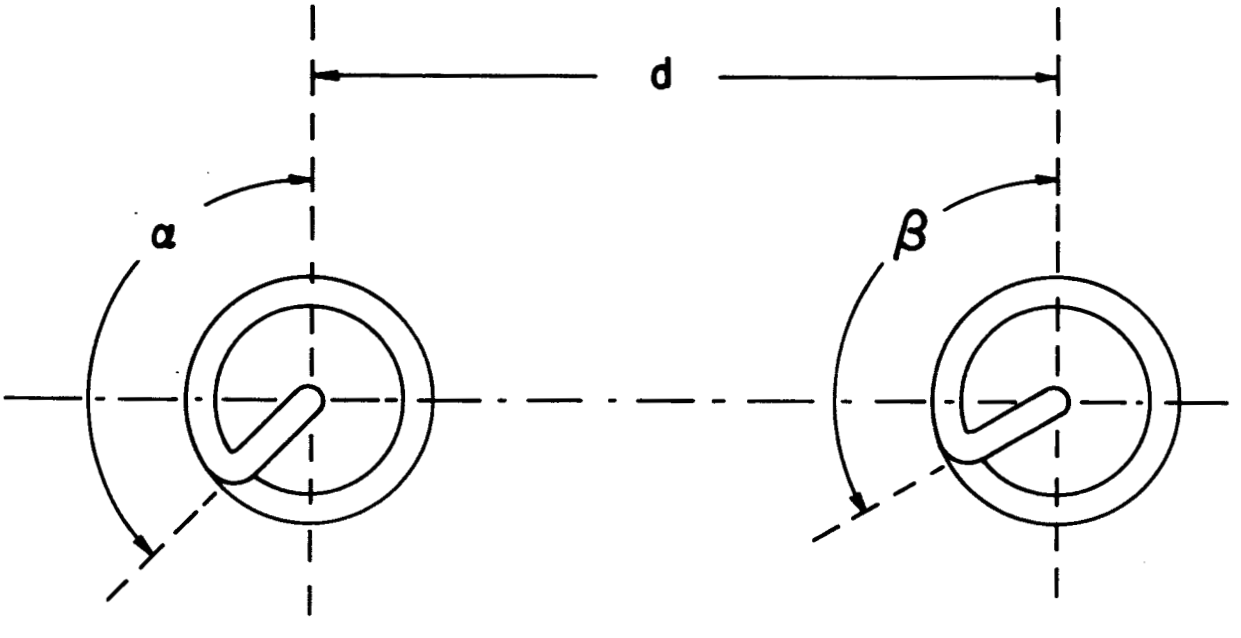

Fig. 30. Definition of angle α and angle β.

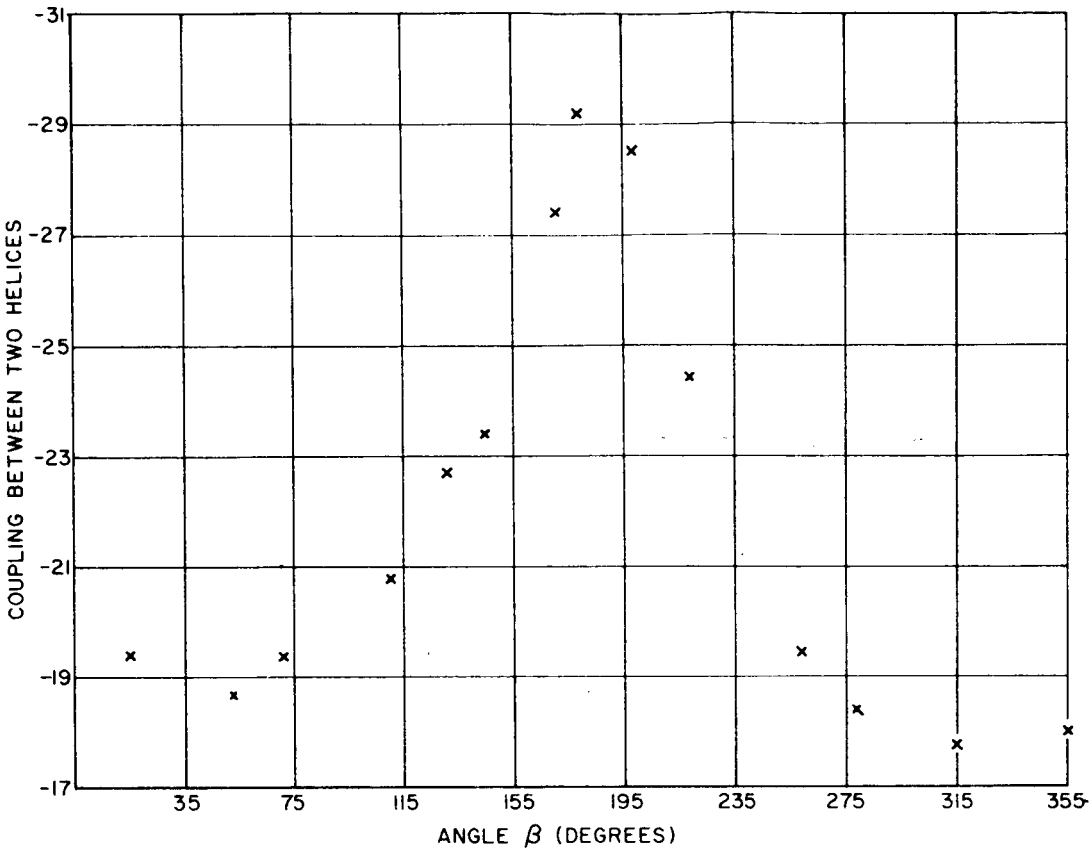

Fig. 31. Coupling between two helices as a function of the angle β.

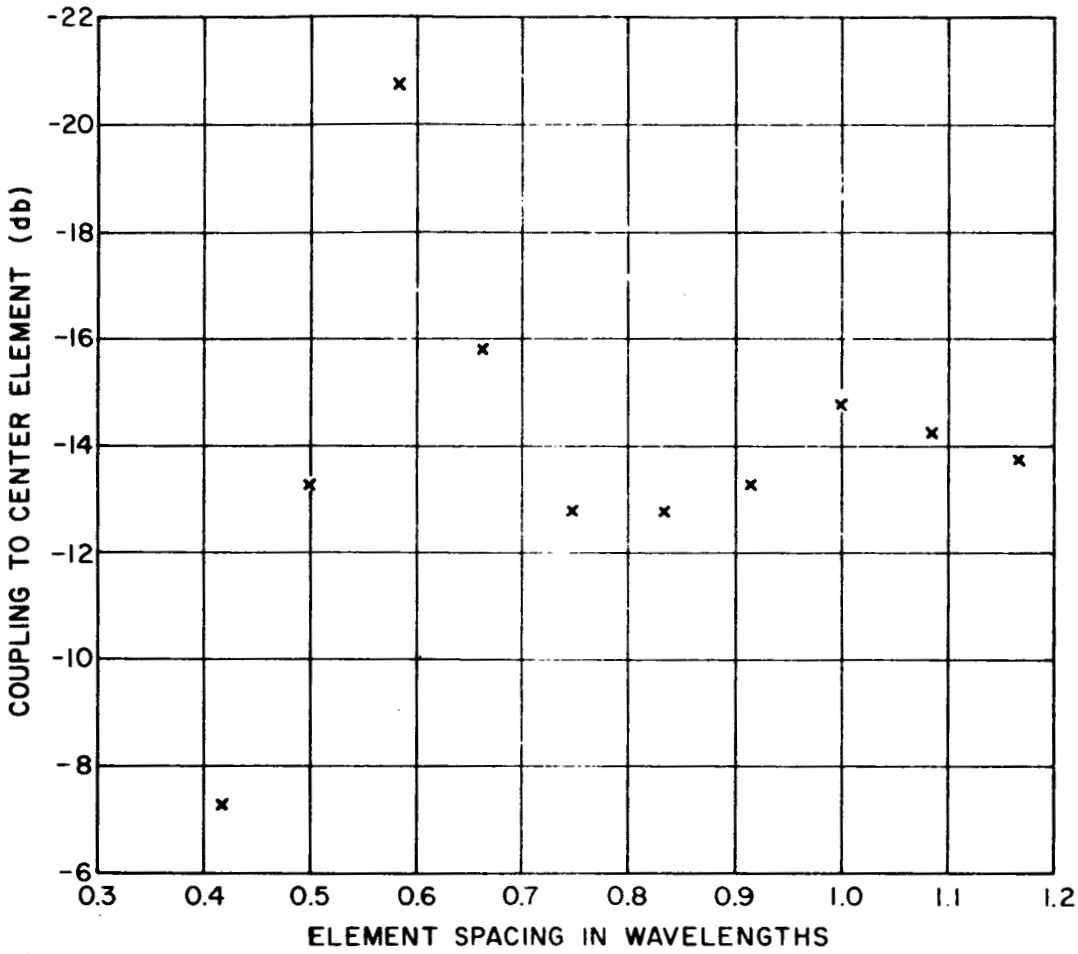

Fig. 32. Power coupled to the center element from the peripheral elements of the planar array.

BIBLIOGRAPHY

[1] Tai, C.T., "The Gain of Uniform Arrays of Isotropic Sources and Dipoles," Report 1522-2, March, 1963, Antenna Laboratory, The Ohio State University Research Foundation; prepared under Contract Number N123(953)-31663A for United States Navy Electronics Laboratory, San Diego, California.

[2] King, H.E., "Directivity of a Broadside Array of Isotropic Radiators," Trans. of PGAP, Vol. AP-7, p. 197, April, 1959.

[3] Sterba, E.J., "Theoretical and Practical Aspects of Directional Transmitting Systems," Proc. IRE, Vol. 19, pp. 1184-1215, July, 1931.

[4] Pomerantz, N., "A Theoretical Investigation of the Directivity of Uniform Linear Arrays," M.Sc. Thesis, Department of Electrical Engineering, The Ohio State University, 1951.

[5] Jasik, H., "Antenna Engineering Handbook," Chapter 5, McGraw-Hill Book Company, Inc., New York, 1961.

[6] Kraus, J.D., Antennas, McGraw-Hill Book Company, Inc., New York, p. 23, 1950.

[7] Kraus, J.D., op. cit., pp. 540-543.

[8] Hamming, R.W., Numerical Methods for Scientists and Engineers," McGraw-Hill Book Company, Inc., New York, pp. 130-132, 1962.

[9] Hildebrand, F.W., Introduction to Numerical Analysis, McGraw-Hill Book Company, Inc., New York, 1956.

[10] Allen, C.C., "Numerical Integration for Antenna Pattern Calculation," IRE Trans. on Antennas and Propagation, pp. 5387-5401, Vol. AP-7, Special Supplement, December, 1959.

[11] Kopal, Z., Numerical Analysis, John Wiley and Sons, Inc., New York, p. 523, 1955.

[12] King, Ronold, "Linear Arrays: Currents, Impedances, and Fields, I," pp. 5440-5467, IRE Trans. on Antennas and Propagation, Vol. AP-7, Special Supplement, December, 1959.

[13] Allen, J.L., "Gain and Impedance Variation in Scanned Dipole Arrays," IRE Trans. on Antennas and Propagation, Vol. AP-10, pp. 566-573, September, 1962.

[14] Hines, J.N., Rumsey, V.H., and Tice, T.E., "On The Design of Arrays," Proc. IRE, Vol. 42, pp. 1262-1267, August, 1954.

[15] Allen, J.L. and Delaney, W.P., "On the Effect of Mutual Coupling on Unequally Spaced Dipole Arrays," IRE Trans. on Antennas and Propagation, pp. 784-785, November, 1962.

[16] Jones, G.C., "Experimental Study of S and X band Helical Aerial Systems," Proc. IEE, Vol. 103B, pp. 764-770, November, 1956.

[17] Hame, T.G., "Microwave Helix Aerials," Electronic Engineering, Vol. 29, pp. 181-183, April 1957.

[18] Kraus, J.D., op. cit., Chapter Seven.

[19] Kiely, D.G., Dielectric Aerials, Chapter Two, John Wiley and Sons, Inc., New York, 1953.

[20] Chu, T.S. and Kilcoyne, N., "The Excitation of a Dielectric-Rod Antenna by a Helix," Report 1035-8, October, 1960, Antenna Laboratory, The Ohio State University Research Foundation; prepared under Contract DA 36-039-sc-84920 for U.S. Army Signal Research and Development Laboratory.

[21] Kieley, D.G., op. cit., p. 110.

[22] Hines, op. cit., p. 1262.

[23] Kraus, J.D., op. cit., p. 43.

[24] Kraus, J.D., op. cit., p. 54.

[25] Tai, C.T., "On the Definition of the Effective Apertures of Antennas," IRE Trans. on Antennas and Propagation, Vol. AP-9, pp. 224-225, March, 1961.

[26] Kraus, John D. and Ksiazek, E., "New Techniques in Radio Astronomy," Electronics, Vol. 26, pp. 149-152, September, 1953.

[27] Ko, H.C. "An Investigation of Galactic Radio Radiation at Frequency of 250 Mc/s," Master of Science Thesis, The Department of Electrical Engineering, The Ohio State University, 1953.

[28] Wylie, C.R., Jr., Advanced Engineering Mathematics, McGraw-Hill Book Company, Inc., p. 430, New York, 1960.

[29] Wylie, C.R., Jr., op. cit., p. 431.

[30] Whiteside, H., "Electromagnetic Field Probes," Cruft Laboratory Technical Report No. 377, Chapt. III, Cambridge, Massachusetts, October 25, 1962.